

Integrated multi-omics and genetic analyses reveal molecular determinants underlying *Arabidopsis snap33* mutant phenotype

Houda Henchiri^{1,2}, Naganand Rayapuram³ , Hanna M. Alhoraibi⁴, José Caius^{1,2}, Christine Paysant-Le Roux^{1,2}, Sylvie Citerne⁵, Herbert Hirt³, Jean Colcombet^{1,2}, Bénédicte Sturbois^{1,2} and Jean Bigeard^{1,2,*} 

¹Université Paris-Saclay, CNRS, INRAE, Université Evry, Institute of Plant Sciences Paris-Saclay (IPS2), 91190 Gif-sur-Yvette, France,

²Université Paris-Cité, CNRS, INRAE, Institute of Plant Sciences Paris-Saclay (IPS2), 91190 Gif-sur-Yvette, France,

³Division of Biological and Environmental Sciences and Engineering, King Abdullah University of Science and Technology, Thuwal 23955, Saudi Arabia,

⁴Department of Biochemistry, Faculty of Science, King Abdulaziz University, 21551 Jeddah, Saudi Arabia, and

⁵Université Paris-Saclay, INRAE, AgroParisTech, Institut Jean-Pierre Bourgin (IJPB), 78000 Versailles, France

Received 29 September 2023; revised 17 November 2023; accepted 9 January 2024.

*For correspondence (e-mail jean.bigeard@univ-evry.fr).

SUMMARY

The secretory pathway is essential for plant immunity, delivering diverse antimicrobial molecules into the extracellular space. *Arabidopsis thaliana* soluble N-ethylmaleimide-sensitive-factor attachment protein receptor SNAP33 is a key actor of this process. The *snap33* mutant displays dwarfism and necrotic lesions, however the molecular determinants of its macroscopic phenotypes remain elusive. Here, we isolated several new *snap33* mutants that exhibited constitutive cell death and H₂O₂ accumulation, further defining *snap33* as an autoimmune mutant. We then carried out quantitative transcriptomic and proteomic analyses showing that numerous defense transcripts and proteins were up-regulated in the *snap33* mutant, among which genes/proteins involved in defense hormone, pattern-triggered immunity, and nucleotide-binding domain leucine-rich-repeat receptor signaling. qRT-PCR analyses and hormone dosages supported these results. Furthermore, genetic analyses elucidated the diverse contributions of the main defense hormones and some nucleotide-binding domain leucine-rich-repeat receptor signaling actors in the establishment of the *snap33* phenotype, emphasizing the preponderant role of salicylic acid over other defense phytohormones. Moreover, the accumulation of pattern-triggered immunity and nucleotide-binding domain leucine-rich-repeat receptor signaling proteins in the *snap33* mutant was confirmed by immunoblotting analyses and further shown to be salicylic acid-dependent. Collectively, this study unveiled molecular determinants underlying the *Arabidopsis snap33* mutant phenotype and brought new insights into autoimmunity signaling.

Keywords: SNAP33, autoimmunity, salicylic acid, *Arabidopsis thaliana*, NLR, ETI, MAPK, PTI, transcriptomics, proteomics.

INTRODUCTION

Plant defense against pathogen attacks relies on constitutive physical and chemical barriers and an inducible immune system. The latter is activated upon recognition of pathogen molecules or plant self molecules by cell-surface and intracellular receptors. The binding of pathogen-associated molecular patterns (PAMPs) or self-damage-associated molecular patterns (DAMPs) by cell-surface pattern-recognition receptors (PRRs) leads to pattern-triggered immunity (PTI) (Bigeard et al., 2015;

Zipfel, 2014). The detection of pathogen effectors by intracellular nucleotide-binding domain leucine-rich-repeat receptors (NLRs) leads to effector-triggered immunity (ETI) (Jones & Dangl, 2006). PRRs can be receptor-like kinases (RLKs) or receptor-like proteins (RLPs), and NLRs are classified as sensor coiled-coil (CC) domain-containing NLRs (CNLs), sensor Toll/interleukin-1 receptor (TIR) domain-containing NLRs (TNLs) or helper HeLo (HET-S and LOPB)-like domain-containing NLRs (helper NLRs) (Saur et al., 2021; Zipfel, 2014). PTI and ETI signaling involve

different actors in their first steps but then share some common mechanisms, such as the production of reactive oxygen species (ROS), the activation of mitogen-activated protein kinases (MAPKs) and defense hormone pathways, and an important transcriptional reprogramming (Lu & Tsuda, 2021). PTI and ETI contribute to immediate defense at pathogen entry sites and can lead to defense priming in distant tissues, a process known as systemic acquired resistance (SAR) (Vlot et al., 2021; Zeier, 2021). It was recently reported that PTI and ETI are actually interdependent and mutually potentiate each other (Ngou, Ahn, et al., 2021; Pruitt et al., 2021; Tian et al., 2021; Yuan et al., 2021).

Some mutants, often referred to as autoimmune mutants, exhibit constitutive activation of immunity, which notably results in stunted growth, macroscopic disease lesions, and even sometimes the death of the plant before flowering (Rodriguez et al., 2016; van Wersch et al., 2016). These genes, whose mutation leads to these autoimmune phenotypes, seem at first sight to be negative regulators of immunity. However, many of them were actually shown to code for gain-of-function NLRs or proteins monitored by NLRs, their depletion thus leading to constitutive activation of immunity (Bruggeman et al., 2015; van Wersch et al., 2016). Genetic analyses of autoimmune mutants have been instrumental to decipher immune signaling pathways.

Membrane trafficking pathways, such as endocytosis and exocytosis, are indispensable for the establishment of an efficient immune response (Gu et al., 2017). Pathogens thus evolved effectors able to manipulate vesicular trafficking as a strategy for successful infection (Petre et al., 2021; Toruño et al., 2016). During defense response, the secretory pathway transports cargoes to the plasma membrane (PM) and extracellular space, such as proteins and metabolites with antimicrobial activities, and callose to reinforce the cell wall (Gu et al., 2017). Vesicles transported for secretion first undergo tethering to the PM, carried out by the exocyst complex, then fusion to the PM, achieved by the assembly of a soluble N-ethylmaleimide-sensitive-factor attachment protein receptor (SNARE) complex (Lipka et al., 2007; Zárský et al., 2013).

The *Arabidopsis thaliana* genome codes for 64 SNARE proteins classified according to their different SNARE domains (Gu et al., 2020). A SNARE complex requires the assembly of an R-SNARE on the vesicle with several Q-SNAREs on the targeted membrane, which together form a Qa-, Qb- and Qc-SNARE four-helix bundle complex (Lipka et al., 2007). In *Arabidopsis*, three genes encode mammal SNAP25-like proteins, which possess both Qb- and Qc-SNARE domains. Among them, SNAP33 is expressed ubiquitously, localizes at the PM and cell plate, and plays a role in cytokinesis together with Qa-SNARE SYP111/KNOLLE and R-SNAREs VAMP721 and VAMP722 (El Kasmi et al., 2013; Heese et al., 2001). Besides, SNAP33 expression is induced notably by

bacterial, fungal, and oomycete pathogens (Wick et al., 2003), and SNAP33 assembles with Qa-SNARE SYP121/PEN1 and R-SNAREs VAMP721 and VAMP722 for focal secretion at fungal entry sites (Kwon et al., 2008; Meyer et al., 2009). SNAP33 can also be associated with several exocyst subunits, including EXO70B1 which contributes to immunity (Pecenková et al., 2011; Zhao et al., 2015). The *snap33* mutant was isolated about 20 years ago and was shown to display dwarfism and necrotic lesions, reminiscent of autoimmune phenotypes (Heese et al., 2001). However, the molecular determinants of *snap33* macroscopic phenotypes remain elusive.

Here, we isolated novel *snap33* mutant alleles and showed that *snap33* is an autoimmune mutant. Using transcriptomic and proteomic approaches, we then report that it displays constitutive expression of numerous defense-related genes and proteins. By targeted genetic analyses, we show that the *snap33* phenotype depends mainly on the salicylic acid (SA) pathway and that some NLR signaling actors contribute to its establishment. Our results also indicate that PTI components are primed in this autoimmune mutant, in part through SA signaling. Overall, these findings reveal key molecular determinants underpinning the *Arabidopsis snap33* mutant phenotype and bring novel insights into autoimmunity signaling.

RESULTS

snap33 mutants exhibit constitutive cell death and H₂O₂ accumulation

The sole *Arabidopsis snap33* mutant described so far was isolated in the Wassilewskija (Ws) ecotype, and will be referred to as *snap33*^{Ws} hereafter (Heese et al., 2001). In order to create a variety of combinatorial mutants for a deeper comprehension of the *snap33* phenotype, we decided to isolate *snap33* mutants within the Col-0 ecotype, as most *Arabidopsis* mutants are available in this genetic background. Five independent T-DNA insertion lines were obtained: SALK_075519 (*snap33-1*), SALK_063806 (*snap33-2*), GABI_094E01 (*snap33-3*), SALK_119791 (*snap33-4*) and SALK_034227 (*snap33-5*) (Figure 1a; Figure S1a). Wild-type (WT) plants out-segregated from *snap33-1*^{+/-} heterozygous mutant (called WT-1) were used as a control in most experiments. A recessive phenotype co-segregated with the T-DNA insertion in the *snap33-1*, *snap33-2*, and *snap33-3* lines, but not in the *snap33-4* and *snap33-5* lines (Figure 1b). The *snap33-1*, *snap33-2*, and *snap33-3* lines exhibited extreme dwarfism, and spontaneous lesion formation, and did not flower under normal growth conditions, similar to the *snap33*^{Ws} phenotype (Figure 1b). RT-PCR analysis of SNAP33 expression in WT-1 plants and *snap33* homozygous mutant plants showed that the *snap33-4* and *snap33-5* lines, with a WT-like phenotype, expressed SNAP33 at similar levels as WT-1, while

snap33-1, *snap33-2* and *snap33-3* lines did not express *SNAP33* (Figure S1b). These results confirm that the severe phenotype is related to *SNAP33* loss of function. The phenotype of *snap33* is reminiscent of autoimmune mutant phenotypes (Bruggeman et al., 2015; van Wersch et al., 2016). In agreement with this, we observed that *snap33* mutants display extensive constitutive cell death and H₂O₂ accumulation (Figure 1c). Because the dwarf phenotype of autoimmune mutants can be partially or totally suppressed by high temperature and/or high humidity, *snap33-1* mutant and WT-1 plants were grown at 30°C under long-day conditions (Figure S1c). The dwarf phenotype of *snap33-1* plants was partially suppressed by high temperature, allowing the mutants to produce some rare seeds. Overall, these results show that *snap33* loss of function mutants are autoimmune mutants.

The *snap33-1* mutant displays constitutive expression of defense-related genes and proteins

To further characterize *snap33* mutants and get a broad picture of the molecular mechanisms associated with their autoimmunity, we compared the transcriptome of the *snap33-1* mutant and WT-1 plants at 5 days, that is, at an early stage of development before the onset of dwarfism and spontaneous lesions, and at 12 days, that is, when the *snap33* characteristic phenotype is well-established (Figure 2a; Figure S2). RNA-seq data indicated that 2591 and 7998 genes were differentially expressed between *snap33-1* and WT-1 5-day-old and 12-day-old seedlings, respectively (P -value <0.05) (Figure 2b–d; Data S1). Among these differentially expressed genes (DEGs), 1662 and 4173 genes were up-regulated at 5 and 12 days, respectively, with 672 and 2015 genes showing at least a two-fold change ($\log_2FC \geq 1$), and 929 and 3825 genes were down-regulated at 5 and 12 days, respectively, with 175 and 954 genes showing at least a two-fold change ($\log_2FC \leq -1$) (Figure 2d). These results show that a massive transcriptional reprogramming occurs in the *snap33-1* mutant, as early as in 5-day-old seedlings, yet no apparent macroscopic phenotype arises at this stage. To obtain an overview of the biological processes affected in the *snap33-1* mutant, we conducted gene ontology (GO) analyses of the DEGs with $|\log_2FC| \geq 1$. Comparison of the up-regulated genes at 5 and 12 days showed an overlap of 288 genes, the GO analysis of which revealed enrichment of biological processes associated with stress response, such as ‘cellular response to hypoxia’, ‘response to wounding’, ‘response to jasmonic acid’, ‘response to salicylic acid’, and ‘defense response’ (Figure 2e; Figure S3). GO analysis of the 384 and 1727 genes that were specifically up-regulated at 5 and 12 days, respectively, also revealed enrichment of biological processes involved in stress response, but with some specificities according to the growth stage, such as the term ‘plant-type hypersensitive

response’ that was specifically enriched at 12 days (Figure S3). We delved deeper into this GO term, revealing that 27 of the 76 genes listed in this GO category were up-regulated in *snap33-1* at 12 days (Figure S4a). These genes are notably associated with SA and SAR (e.g., *SARD1*, *CBP60g*, *PBS3*, *NPR1*, and *FMO1*) and R protein signaling (e.g., *EDS1*, *PAD4*, *NDR1*, and *ADR1*) (Figure S4b). Regarding the down-regulated genes, comparison between the two growth stages showed an overlap of 44 genes, whose GO analysis revealed essentially an enrichment of the terms ‘plant-type cell wall organization’ and ‘wax biosynthetic process’ (Figure S5). The sets of 131 and 910 genes that were specifically down-regulated at 5 and 12 days, respectively, were both enriched in terms associated with growth and development, with notably again terms related to cell wall organization (Figure S5). One of the main noticeable specificities between these two sets of genes is exemplified by the terms ‘brassinosteroid homeostasis’ and ‘brassinosteroid biosynthetic process’ which are specifically enriched at 5 days.

The RNA-seq data revealed major changes in gene expression in the *snap33-1* mutant, especially at 12 days. Since proteins are the main executors of biological processes, we also compared the proteome of *snap33-1* mutant and WT-1 plants at 12 days. Data-independent acquisition mass spectrometry (DIA-MS) analysis allowed the identification and quantification of about 8700 protein groups (Figure S6 and Data S2), representing 56.2% of the mass spectral library used for the analysis and 31.7% of the Arabidopsis predicted proteome (Methods S4) (Zhang et al., 2019). In this study, 1129 unique proteins were identified as differentially expressed proteins (DEPs) between the *snap33-1* mutant and WT-1 12-day-old seedlings (q -value <0.01) (Data S2). Among these DEPs, 605 and 524 were up-regulated and down-regulated in the *snap33-1* mutant, respectively, with 447 and 169 showing at least a more stringent 1.5-fold change ($|\log_2FC| \geq 0.58$), respectively (Figure 3a,b; Data S2). GO analyses of the DEPs with $\log_2FC \geq 0.58$ indicated that up-regulated proteins were enriched in processes associated with stress response, the five most significant terms being ‘systemic acquired resistance’, ‘response to oxidative stress’, ‘response to wounding’, ‘defense response to bacterium’, and ‘response to jasmonic acid’ (Figure 3c). Conversely, GO analyses of the DEPs with $\log_2FC \leq -0.58$ showed that down-regulated proteins were predominantly associated with metabolic processes, such as ‘hydrogen peroxide catabolic process’, ‘thiamine biosynthetic process’, ‘cellular oxidant detoxification’, and ‘photosynthesis’ (Figure S7).

A positive correlation between mRNA and protein levels is usually observed (Mergner et al., 2020). To assess this correlation in *snap33-1* 12-day-old mutant seedlings, we compared the 2969 DEGs with $|\log_2FC| \geq 1$ (P -value <0.05) and 616 DEPs with $|\log_2FC| \geq 0.58$ (q -value

4 Houda HENCHIRI et al.

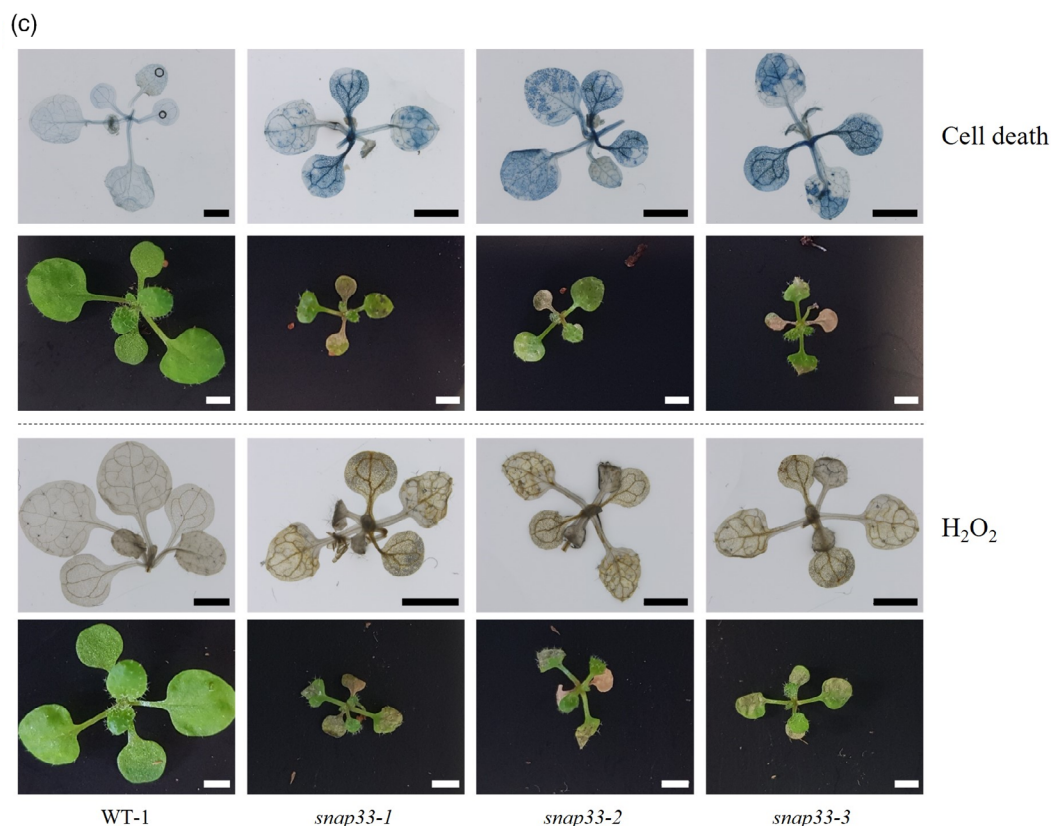
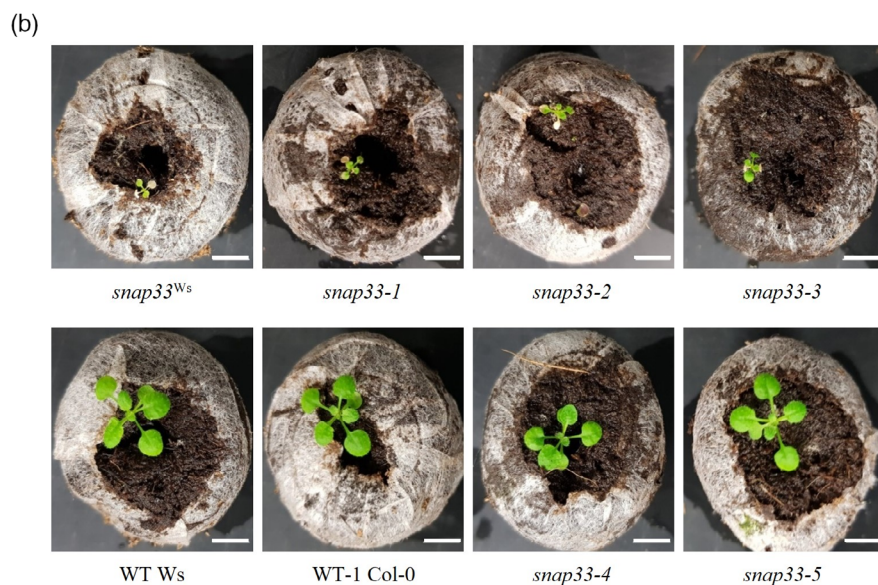
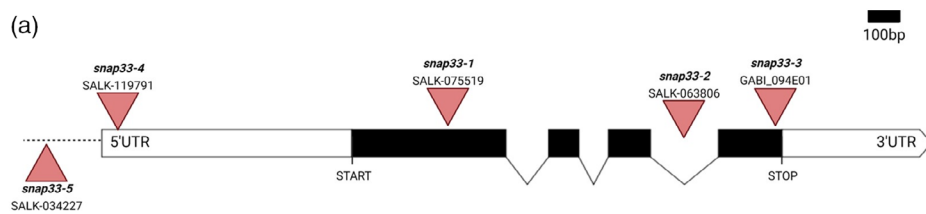


Figure 1. New *snap33* T-DNA mutants were isolated, several of which exhibited dwarfism, cell death, and H₂O₂ accumulation.

(a) Schematic representation of *SNAP33* genomic region (2585 bp) with the location of the T-DNA insertion in the *snap33-1*, *snap33-2*, *snap33-3*, *snap33-4*, and *snap33-5* mutants. Exons are represented as black boxes, 5'UTR and 3'UTR as white boxes, introns as short lines, and the START and STOP codons are indicated. Triangles indicate the sites of T-DNA insertions.

(b) Representative pictures of 21-day-old seedlings of indicated genotypes. Scale bars represent 1 cm.

(c) 21-day-old *snap33-1*, *snap33-2* and *snap33-3* seedlings display cell death (upper pictures) and H₂O₂ accumulation (lower pictures) as revealed by trypan blue and DAB stainings, respectively. Cell death appears as dark blue patches and H₂O₂ accumulation appears as brown patches in the *snap33* mutants. Associated photographs show unstained seedlings. Scale bars represent 2 mm. Three biological replicates were carried out, with similar results. In each biological replicate, three plants of each genotype were stained.

<0.01). An overlap of 247 DEGs/DEPs was found which showed a high positive correlation between transcript and protein fold-change levels with a Pearson estimated measure of association $r = 0,75$ (P -value = $1.95e^{-46}$) (Figure 3d). The heatmap of the log₂FC of these 247 DEGs/DEPs similarly revealed this high positive correlation (Figure S8).

The *snap33-1* mutant phenotype mainly depends on the SA pathway

One of the key features revealed by both the RNA-seq and DIA-MS data was the enrichment of defense hormone-related processes in the *snap33-1* mutant. Numerous up-regulated genes were indeed associated with the biosynthesis and response to SA and JA, and a lesser extent with those of ethylene (ET) (Figure 2e; Figure S3), and several up-regulated proteins were involved in the biosynthesis of these hormones (Figure S9). These three hormones regulate specific signaling pathways while also engaging in crosstalk, collectively forming an intricate signaling network (Aerts et al., 2021; Altmann et al., 2020). We confirmed by qRT-PCR that genes involved in SA pathway activation (*CBP60g*), synthesis (*EDS5*), signaling (*NPR1*) and response markers (*PR1* and *PR2*), and genes involved in JA-ET signaling (*ORA59* and *ERF1*) and response marker (*PDF1.2*) were all up-regulated in the independent *snap33-3* mutant (Figure 4a). The transcript fold-changes of these marker genes observed by RNA-seq and qRT-PCR were similar, which overall validated the RNA-seq dataset. Additionally, the up-regulation of these hormone marker genes suggested that the corresponding hormones accumulated in the *snap33* mutant. We thus measured the levels of SA, its storage form SA beta-glucoside (SAG), JA, and ET, showing their elevated accumulation in *snap33* mutant plants (Figure 4b). To investigate the contribution of these three defense hormones in the phenotype of the *snap33* mutant, we crossed the *snap33-1* mutant with *sid2-2*, a mutant largely impaired in SA biosynthesis (Dewdney et al., 2000; Wildermuth et al., 2001), *coi1-34*, a mutant of the JA receptor (Acosta et al., 2013), and *ein2-1*, a mutant impaired in ET signaling (Alonso et al., 1999; Guzmán & Ecker, 1990). By measuring the rosette fresh weight (FW) as readout of the genetic effects of these hormone mutants, we found that the *sid2-2* mutation slightly suppressed the phenotype of *snap33-1*, while *coi1-34* and *ein2-1* mutations had no effect

on the *snap33-1* phenotype (Figure 5a,b; Figure S10a). Because SA, JA, and ET may display antagonistic, synergistic, and additive effects, we also produced *snap33-1 sid2-2 coi1-34*, *snap33-1 sid2-2 ein2-1*, and *snap33-1 coi1-34 ein2-1* combinatorial mutants. The results indicated a tendency for a synergistic effect of *coi1-34* with *sid2-2* to suppress *snap33-1* phenotype, as in average the rosette FW of *snap33-1 sid2-2 coi1-34* plants was higher than the one of *snap33-1 sid2-2* plants, although the statistical test did not show a significant difference between them (Figure 5a,b; Figure S10a). Conversely, there was a tendency for an antagonistic effect of *ein2-1* with *sid2-2*, as in average the rosette FW of *snap33-1 sid2-2 ein2-1* plants was lower than the one of *snap33-1 sid2-2* plants, although the statistical test did not show a significant difference. In addition, no suppression of the *snap33-1* phenotype was observed with the combined *coi1-34* and *ein2-1* mutations. Ultimately, we created the *snap33-1 sid2-2 coi1-34 ein2-1* quadruple mutant and compared it to previously characterized mutants, using a larger sample size. The results demonstrated that *snap33-1 sid2-2 coi1-34* triple mutant plants indeed exhibited a stronger reversion of the *snap33-1* phenotype compared to *snap33-1 sid2-2* double mutants. However, it is worth noting that the *ein2-1* mutation reduces this phenotypic reversion in the *snap33-1 sid2-2 coi1-34 ein2-1* quadruple mutant, aligning with the trend previously observed in the *snap33-1 sid2-2 ein2-1* triple mutant (Figure 5a,c; Figure S10b). In conclusion, only the *sid2-2* mutation, i.e., the SA pathway, had a significant suppressive effect on the *snap33-1* phenotype, but with synergistic and antagonistic effects of *coi1-34* and *ein2-1* mutations, respectively.

Besides the partial suppression of the *snap33-1* mutant dwarfism by the *sid2-2* mutation, the necrotic lesions were still present in five-week-old *snap33-1 sid2-2* plants, similarly as in *snap33-1* plants (Figure 5a). However, the formation of these necrotic lesions was delayed, as they were hardly visible in 21-day-old plants, and in line with this, the cell death and H₂O₂ accumulation were reduced to the same levels as in WT-1 and *sid2-2* seedlings (Figure 5d). Moreover, *PR1* expression exhibited quite basal levels in 12-day-old *snap33-1 sid2-2* mutant plants (Figure 5e).

In addition to the enrichment of defense hormone-related processes in the *snap33-1* mutant, the RNA-seq and

6 Houda Henchiri et al.

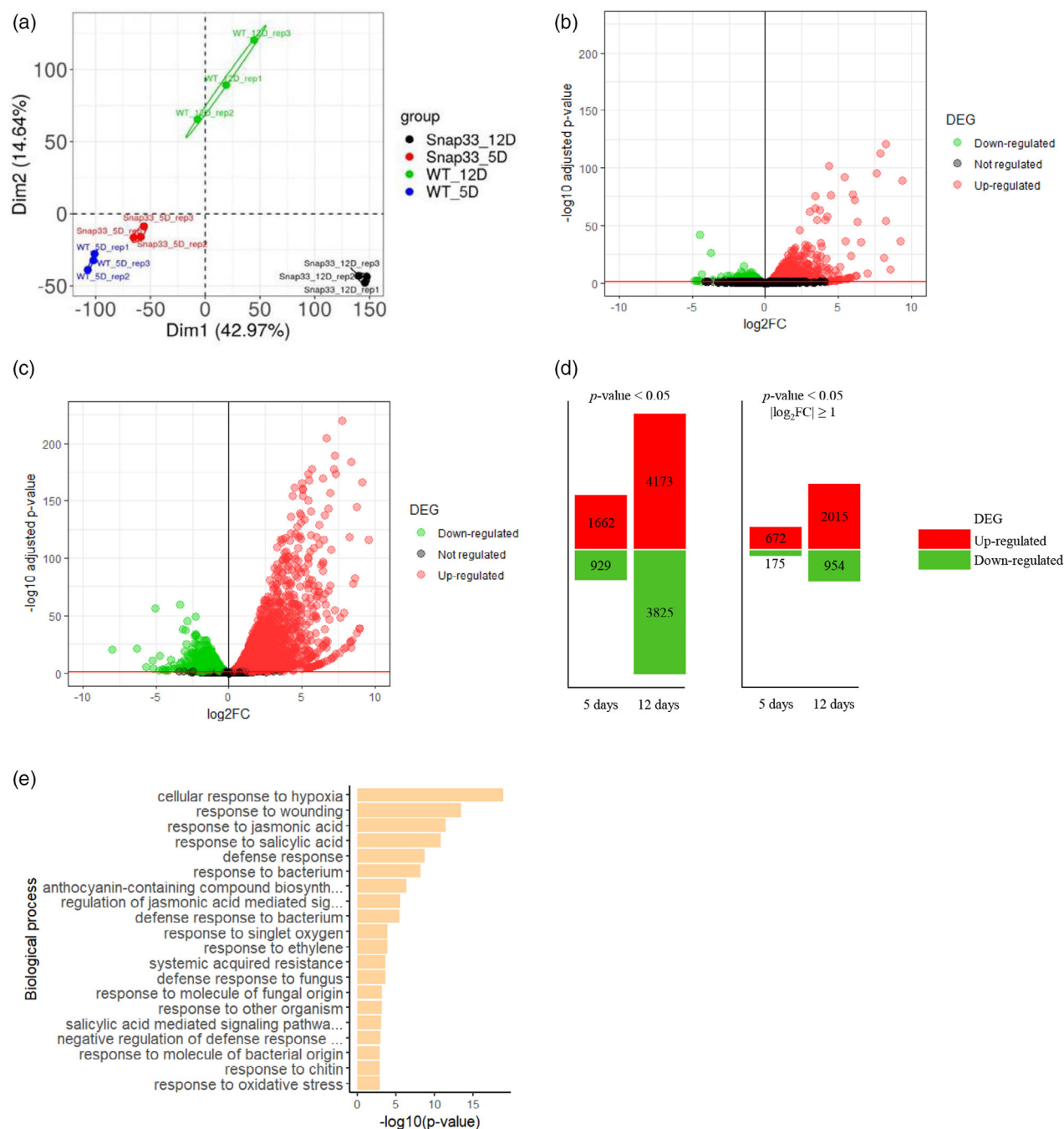


Figure 2. RNA-sequencing (RNA-seq) analyses of 5-day-old and 12-day-old WT-1 and *snap33-1* mutant seedlings.

(a) Normalized counts of RNA-seq data were submitted to principal component analysis (PCA). Each point represents an RNA-seq sample, i.e. a genotype x age combination. Sample groups are visualized by different colors, as indicated in the legend. The PCA indicates that the different biological repeats of each condition were highly similar, showing the high reproducibility of the approach and that *snap33-1* and WT-1 samples showed the most remarkable difference at 12 days of growth, as expected from their corresponding macroscopic phenotype. In this study, 12D and 5D, respectively, stand for 12-day-old and 5-day-old seedlings.

(b) Volcano-plot of DEGs (P -value < 0.05) at 5 days.

(c) Volcano-plot of DEGs (P -value < 0.05) at 12 days.

(d) Schematic view of up-regulated and down-regulated DEGs identified at 5 and 12 days with P -value < 0.05 , and among them DEGs with $|\log_2FC| \geq 1$.

(e) GO enrichment analyses of biological processes among the 288 DEGs commonly up-regulated in *snap33-1* at 5 and 12 days. The top 20 most significant categories are represented on the vertical axis and the horizontal axis represents the $-\log_{10}(P\text{-value})$.

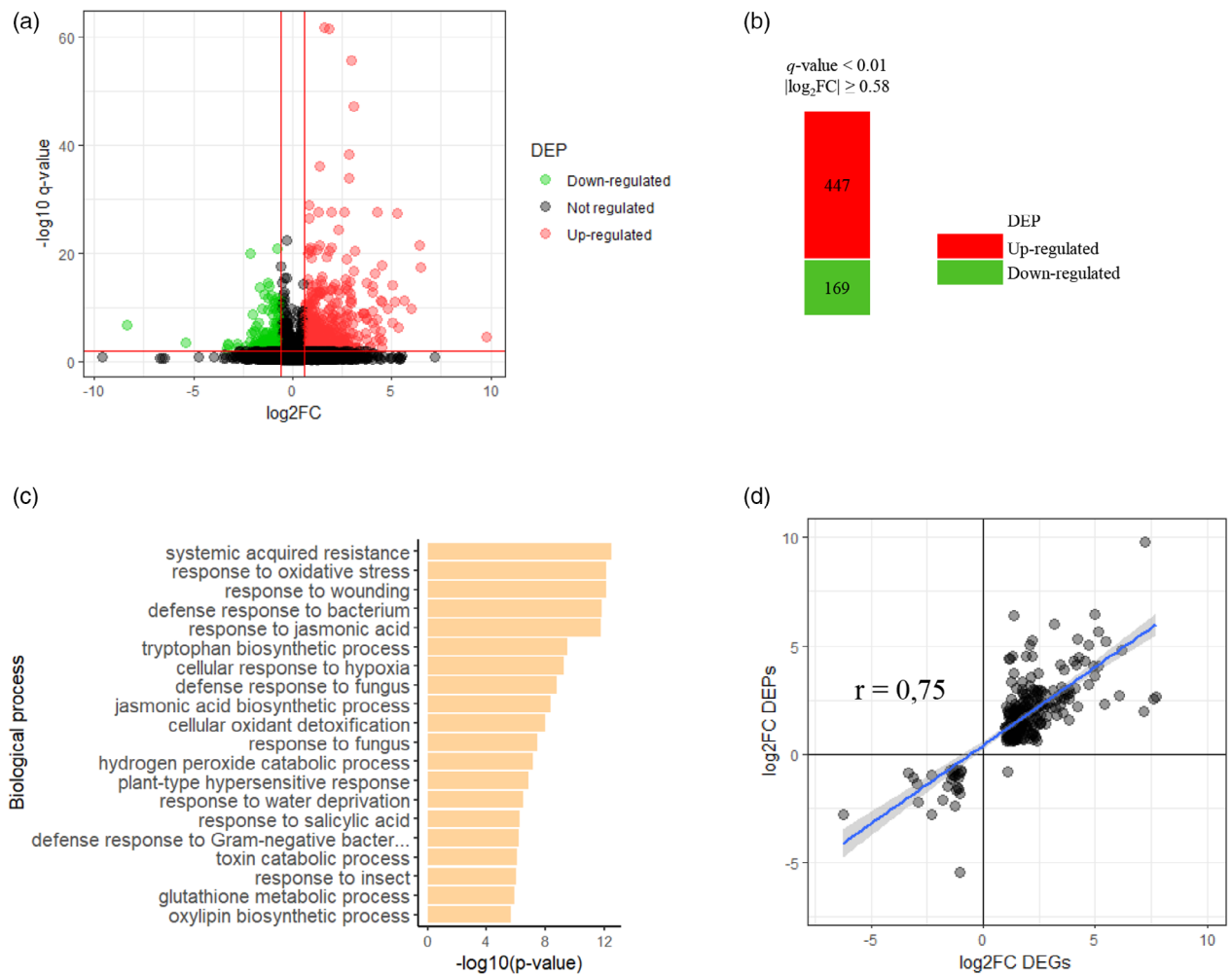


Figure 3. DIA-MS analyses of 12-day-old WT-1 and *snap33-1* mutant seedlings, and comparison to RNA-seq results.

(a) Volcano-plot of DEPs ($q\text{-value} < 0.01$ and $|\log_2 FC| \geq 0.58$).

(b) Schematic view of up-regulated and down-regulated DEPs identified at 12 days with $q\text{-value} < 0.01$ and $|\log_2 FC| \geq 0.58$.

(c) GO enrichment analyses among the 447 DEPs up-regulated in *snap33-1*. The top 20 most significant categories are represented on the vertical axis and the horizontal axis represents the $-\log_{10}(P\text{-value})$.

(d) Scatter-plot of the overlap of 247 DEGs/DEPs from the sets of DEGs with $|\log_2 FC| \geq 1$ ($P\text{-value} < 0.05$) and DEPs with $|\log_2 FC| \geq 0.58$ ($q\text{-value} < 0.01$). The regression line is indicated in blue and the confidence interval in gray. r denotes the estimated Pearson's correlation ($P\text{-value} = 1.95e^{-46}$).

DIA-MS data also revealed the involvement of SAR (Figures 2e and 3c; Figure S3). Together with SA, N-hydroxypipicolinic acid (NHP) is a critical mobile signal for the establishment of SAR in plants (Chen et al., 2018; Hartmann et al., 2018). We confirmed by qRT-PCR that the expression of *ALD1* and *FMO1*, two key genes involved in NHP biosynthesis, were up-regulated in the *snap33-3* mutant (Figure 5f). To evaluate how SAR contributes to the phenotype of *snap33* mutant, we crossed *snap33-1* with *fmo1-1*, a mutant impaired in NHP biosynthesis (Bartsch et al., 2006). We found that *fmo1-1* slightly suppressed the phenotype of *snap33-1*, similar to the *sid2-2* mutation (Figure 5g,h; Figure S10c). Given the importance of both SA and NHP for SAR implementation, we also produced *snap33-1 sid2-2 fmo1-1* triple mutant plants that exhibited

an increased reversion of the *snap33-1* phenotype compared to the two double mutants, suggesting an additive/synergistic effect of SA and NHP (Figure 5g,h; Figure S10c).

SA is produced via two distinct pathways, the isochorismate (IC) pathway and the phenylalanine ammonia-lyase (PAL) pathway (Ding & Ding, 2020) (Figure 6a). The IC pathway accounts for most of the SA production, and in this pathway, isochorismate synthase 1 (ICS1)/SID2 has a major role compared to its homolog ICS2. The *sid2-2* mutation thus largely impairs the biosynthesis of SA (Nawrath & Métraux, 1999). Nonetheless, given the weak suppression of the *snap33-1* phenotype by the *sid2-2* mutation (Figure 5a–c,g,h), we wondered whether SA produced via the above-mentioned alternative pathways could contribute to the observed phenotype. We thus crossed *snap33-1*

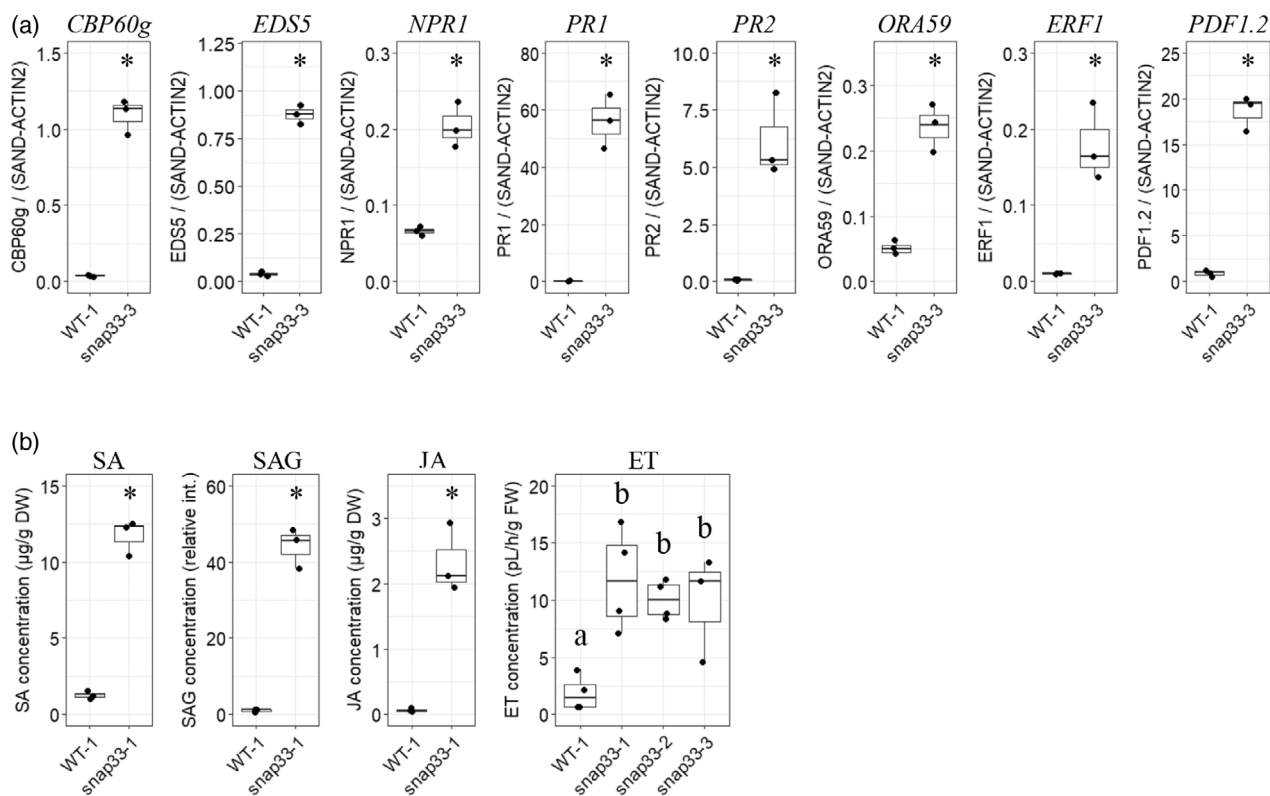


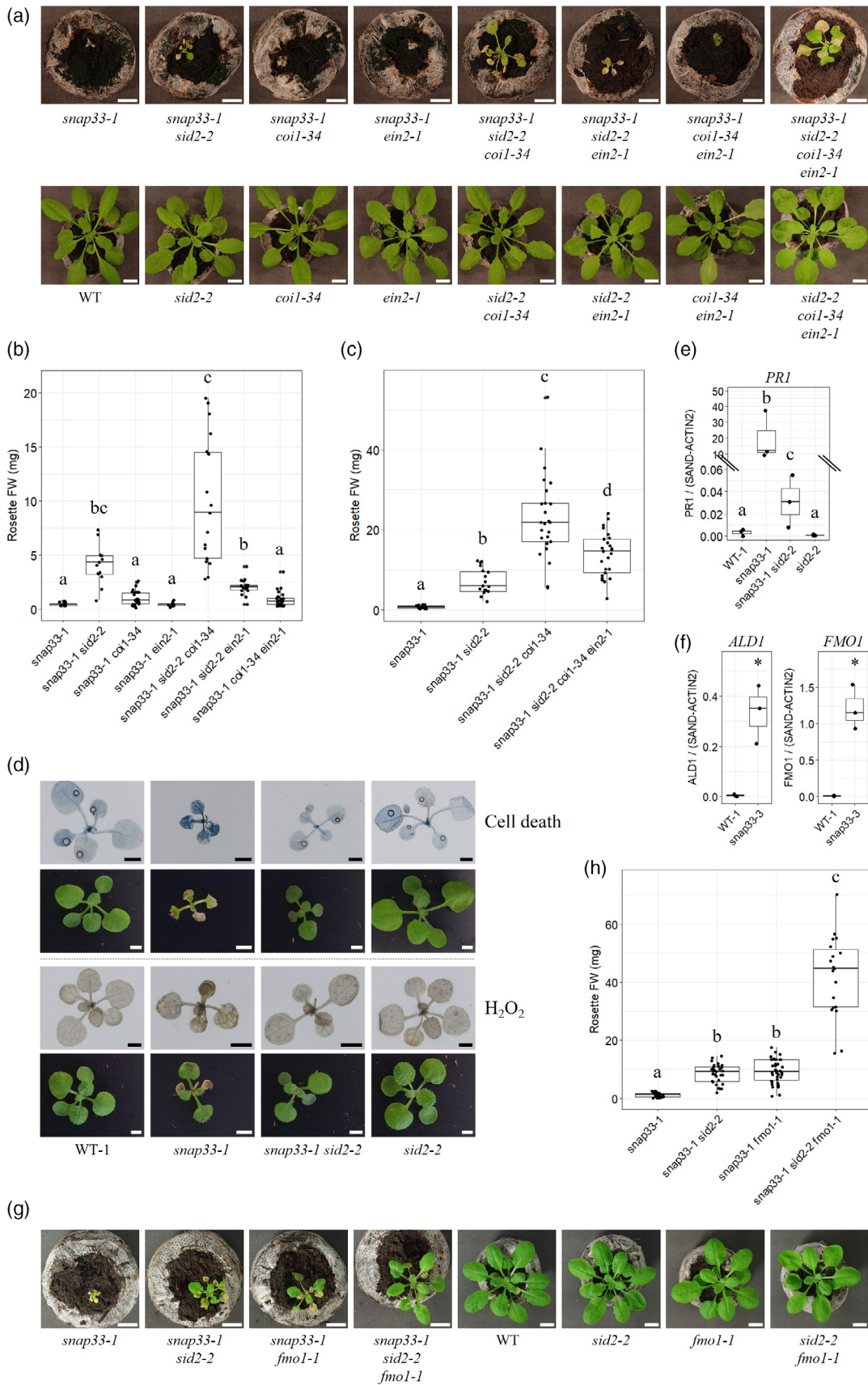
Figure 4. Genes involved in SA, JA, and ET synthesis and signaling are up-regulated in *snap33* mutants, and these hormones exhibit elevated accumulation. (a) qRT-PCR analyses were carried out to measure the expression of the indicated transcripts in WT-1 and *snap33-3* mutant seedlings. The values represent the fold-changes in comparison to the *SAND* and *ACTIN2* reference transcripts. Three independent biological repeats were performed. The non-parametric Wilcoxon rank sum test (or Mann-Whitney U test) was used to analyze the data, and P -value < 0.05 indicated a statistical difference represented by an asterisk. (b) Quantifications of SA, SAG, and JA in WT-1 and *snap33-1* mutant seedlings were carried out by UPLC-MS/MS analyses. Three independent biological repeats were performed. Data were analyzed with the Wilcoxon rank sum test, and P -value < 0.05 indicated a statistical difference represented by an asterisk. ET was quantified in WT-1 and three independent *snap33* mutants. Four independent biological repeats were performed (except three for *snap33-3*). Multiple comparisons were tested with the non-parametric two-sided Tukey test with a confidence level set to 95% using the nparcomp package in R. Different letters above box plots indicate a statistical difference (P -value < 0.05) between the corresponding genotypes. DW: dry weight; FW: fresh weight; int.: intensity.

mutant with *pbs3-2*, a mutant impaired in the production of SA from the IC pathway (Nobuta et al., 2007), and with a line ectopically expressing salicylate hydroxylase NahG (*35S::NahG*), a bacterial enzyme which converts SA to catechol (Lawton et al., 1995). We found that the *snap33-1*

mutant phenotype was slightly suppressed by the *pbs3-2* mutation, similarly but unexpectedly a bit less than the *sid2-2* mutation, and was strongly suppressed by NahG ectopic expression (Figure 6b,c; Figure S11a). Despite the strong reversion effect of NahG expression, *snap33-1 35S::*

Figure 5. *snap33-1* mutant phenotype mainly depends on SA phytohormone.

(a) Representative pictures of 35-day-old plants of indicated genotypes assayed in experiments represented in panels (b) and (c). Scale bars represent 1 cm. (b) Rosette fresh weight (FW) of 35-day-old plants ($n = 9-29$). (c) Rosette FW of 35-day-old plants ($n = 17-25$). (d) Representative pictures of 21-day-old seedlings stained with trypan blue (top panel, cell death) and DAB (lower panel, H_2O_2). Cell death appears as dark blue patches and H_2O_2 accumulation appears as brown patches. Associated photographs show unstained seedlings. Scale bars represent 2 mm. Three biological replicates were carried out, with similar results. In each biological replicate, three plants of each genotype were stained. (e,f) qRT-PCR analyses carried out to measure the expression of *PR1* (e), and *ALD1* and *FMO1* (f) transcripts in 12-day-old seedlings of indicated genotypes. The values represent the fold-changes in comparison to the *SAND* and *ACTIN2* reference transcripts. Three independent biological repeats were performed. For (e), multiple comparisons were tested with the non-parametric two-sided Tukey test with a confidence level set to 95% using the nparcomp package in R. Different letters above box plots indicate statistical difference (P -value < 0.05) between the corresponding genotypes. For (f), the Wilcoxon rank sum test was used to analyze the data, and P -value < 0.05 indicated a statistical difference represented by an asterisk. (g) Representative pictures of 35-day-old plants of indicated genotypes. Scale bars represent 1 cm. (h) Rosette FW of 35-day-old plants ($n = 19-36$). (b,c,h) Multiple comparisons were tested with the Kruskal-Wallis rank sum test followed by Dunn post hoc tests using the Benjamini-Hochberg method for P -values adjustment. Different letters above box plots indicate a statistical difference (P -value < 0.05) between the corresponding genotypes.



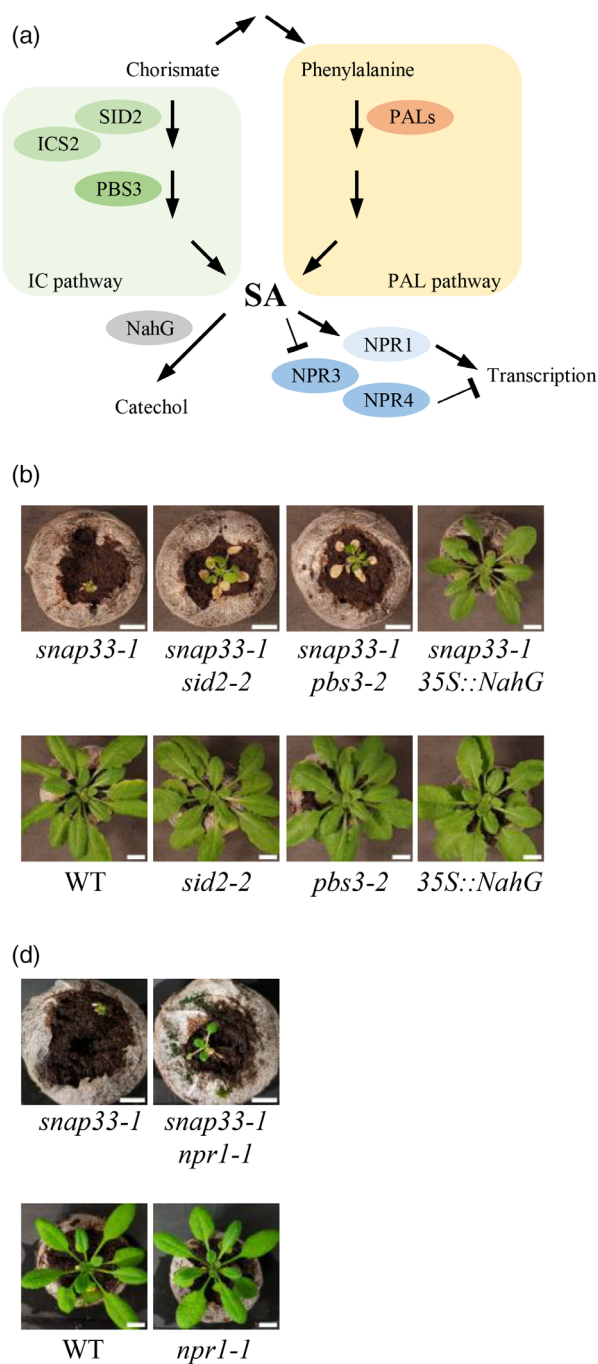


Figure 6. Involvement of key actors of SA synthesis and perception in the establishment of *snap33-1* mutant phenotype.

(a) Scheme of SA synthesis, perception, and degradation.

(b) Representative pictures of 35-day-old plants of indicated genotypes. Scale bars represent 1 cm.

(c) Rosette fresh weight (FW) of 35-day-old plants ($n = 24\text{--}45$). Multiple comparisons were tested with the Kruskal–Wallis rank sum test followed by Dunn post hoc tests using the Benjamini–Hochberg method for P -values adjustment. Different letters above box plots indicate a statistical difference (P -value < 0.05) between the corresponding genotypes.

(d) Representative pictures of 35-day-old plants of indicated genotypes. Scale bars represent 1 cm.

(e) Rosette FW of 35-day-old plants ($n = 34\text{--}42$). The Wilcoxon rank sum test was used to analyze the data, and P -value < 0.05 indicated a statistical difference represented by an asterisk.

NahG rosette FW was still significantly lower than the control genotype rosette FW (Figure S11a). These results showed that the *snap33-1* mutant phenotype mainly

depends on the SA pathway, and suggested that both the IC and PAL pathways contribute to SA signaling in the *snap33* autoimmune mutant.

SA is perceived by six NPR receptors (Ngou, Jones, & Ding, 2021). It was recently shown that SA strengthens the transcriptional activation function of NPR1 and suppresses the transcriptional repression function of NPR3 and NPR4 (Ding et al., 2018) (Figure 6a). To assess the contribution of *NPR1* to the *snap33-1* phenotype, we crossed *snap33-1* with the *npr1-1* loss-of-function mutant (Cao et al., 1997). We found that the *npr1-1* mutation slightly suppressed the phenotype of the *snap33-1* mutant (Figure 6d,e; Figure S11b), and the suppression level was seemingly similar to the one observed with the *sid2-2* and *pbs3-2* mutations (Figures 5a–c,g,h and 6b,c). Taken together with the phenotype of *snap33-1 35S::NahG* mutant plants, these results suggested that *NPR1* indeed contributes to the phenotype of *snap33-1* mutant plants, but also that *NPR1*-independent, most likely *NPR3/NPR4*-dependent signaling pathways also play a role in the *snap33-1* phenotype.

Some NLR signaling components contribute to the *snap33-1* mutant phenotype

Autoimmunity is most often due to the constitutive activation of an NLR or to the loss of function of a negative regulator of immunity (van Wersch et al., 2016). Given the known function of SNAP33 as a Qbc-SNARE involved in exocytosis, we hypothesized that *SNAP33* mutation would result in the constitutive activation of an NLR, that is, that SNAP33 would be guarded by a sensor NLR. In this context, the lipase-like domain and EP-domain-containing protein EDS1, together with the closely related PAD4 and SAG101, interacts with ADR1 and NRG1 helper NLRs to propagate signaling downstream TNLs (Lapin et al., 2020; Ngou et al., 2022). EDS1 was also reported to signal downstream some non-TNL receptors (Bhandari et al., 2019; Venugopal et al., 2009). In addition, the integrin-like protein NDR1 may be necessary to transduce CNL-triggered signaling, although some CNLs can turn on defense irrespective of NDR1 (Kapos et al., 2019). All these ETI signaling genes were up-regulated in 12-day-old *snap33-1* seedlings (Data S1) which we confirmed by qRT-PCR for the tested ones in *snap33-3* (Figure 7a). To evaluate the contribution of NDR1 and EDS1 to the *snap33-1* phenotype, we crossed *snap33-1* with *ndr1-1* and *eds1-2* loss-of-function mutants and also generated the *snap33-1 ndr1-1 eds1-2* triple mutant (Bartsch et al., 2006; Century et al., 1997). We found that both *eds1-2* and *ndr1-1* mutations slightly suppressed the *snap33-1* phenotype, similarly but apparently with a better effect in the case of *eds1-2* mutation, and the suppression was even greater in the *snap33-1 ndr1-1 eds1-2* triple mutant (seemingly similar to *snap33-1 sid2-2* double mutant), suggesting an additive/synergistic effect of *ndr1-1* and *eds1-2* mutations (Figure 7b,c; Figure S12a). Overall, these results showed the involvement of some key NLR signaling actors in the establishment of the *snap33-1* mutant phenotype and thus

suggested that one or several NLR proteins may also be implicated.

Interestingly, SNAP33 interacts with some protein partners whose disruption leads to R protein signaling. Indeed, SNAP33 interacts with the exocyst tethering factor EXO70B1, and the *exo70B1* mutant exhibits an autoimmune phenotype due to activation of TIR-NBS2 (TN2), an atypical TNL lacking the LRR domain, and activation of CPK5 CDPK (Liu et al., 2017; Zhao et al., 2015). This TN2-mediated signaling also requires the helper NLRs ADR1s, which are EDS1 signaling partners (Wang et al., 2021). *TN2* transcript was solely detected by RNA-seq in 12-day-old *snap33-1* mutant, and CPK5 was up-regulated at the transcript and protein levels by factors of about 1.5 and 2, respectively (Data S1 and S2). In addition, SNAP33 also interacts with the Qa-SNARE/syntaxin SYP121/PEN1 to form a SNARE complex together with the VAMP721 and VAMP722 R-SNAREs (Kwon et al., 2008). While the *syp121* single mutant does not display a marked phenotype, the *syp121 syp122* double mutant exhibits dwarfism and autoimmunity, which can be suppressed by mutation of *AMSH3*, a deubiquitinase whose function is necessary for immunity mediated by some CNLs (Schultz-Larsen et al., 2018; Zhang et al., 2007). To investigate the contribution of CPK5, TN2, and *AMSH3* in the phenotype of the *snap33* mutant, we crossed the *snap33-1* mutant with *cpk5-1*, *tn2-1* and *amsh3-4* mutants, and generated the *snap33-1 tn2-1 amsh3-4* triple mutant (Boudsocq et al., 2010; Schultz-Larsen et al., 2018; Zhao et al., 2015). We found that the *tn2-1* mutation had no effect but that *cpk5-1* and *amsh3-4* mutations led to a slight suppression of the *snap33-1* phenotype (Figure 7d–g; Figure S12b,c). Besides, the *snap33-1 tn2-1 amsh3-4* triple mutant was not statistically different from *snap33-1 amsh3-4* double mutant plants, although a tendency for a synergistic effect of the *tn2-1* mutation was observed. Overall, these results suggested the implication of some unknown CNL(s) linked to *AMSH3*, in agreement with the effect of the *ndr1-1* mutation observed above, and of the TN2-CPK5 module.

Considering the moderate suppression of the *snap33-1* phenotype by the combined loss-of-function mutations of *NDR1* and *EDS1* on one hand, and of *TN2* and *AMSH3* on the other hand, compared to the strong effect of *NahG* expression, we suggest that multiple NLRs could actually contribute to the *snap33* mutant phenotype, with at least one of them being independent of *NDR1* and *EDS1* signaling. As NLR activation leads to the up-regulation of other NLR genes, it was proposed that it could favor the ulterior activation of those NLRs (Ngou, Jones, & Ding, 2021). Besides, the sole up-regulation, for instance, of *AT3G04220*, *AT4G11170*, and *AT2G32140* NLR genes is sufficient to activate the SA pathway (Lang et al., 2022; Tian et al., 2021). Therefore, we examined our RNA-seq and DIA-MS data for the presence of up-regulated NLR genes

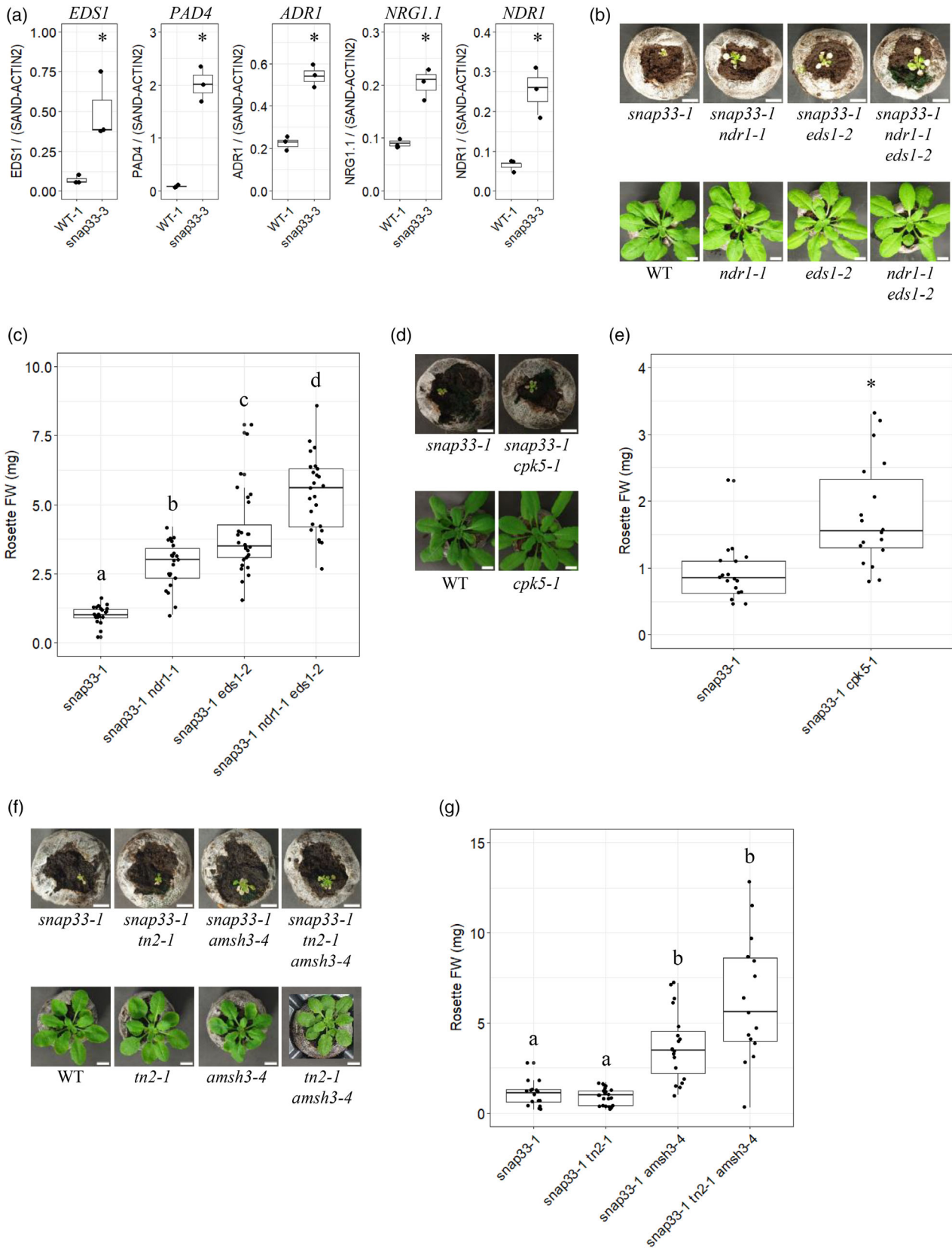


Figure 7. *snap33-1* mutant phenotype depends on multiple NLR signaling pathways.

- (a) qRT-PCR analyses were carried out to measure the expression of *NLR* signaling genes in 12-day-old WT-1 and *snap33-3* mutant seedlings. The values represent the fold-changes in comparison to the *SAND* and *ACTIN2* reference transcripts. Three independent biological repeats were performed.
- (b) Representative pictures of 35-day-old plants of indicated genotypes. Scale bars represent 1 cm.
- (c) Rosette fresh weight (FW) of 35-day-old plants ($n = 21$ – 28).
- (d) Representative pictures of 35-day-old plants of indicated genotypes. Scale bars represent 1 cm.
- (e) Rosette FW of 35-day-old plants ($n = 18$).
- (f) Representative pictures of 35-day-old plants of indicated genotypes. Scale bars represent 1 cm.
- (g) Rosette FW of 35-day-old plants ($n = 15$ – 23).
- (a,e) The Wilcoxon rank sum test was used to analyze the data, and P -value < 0.05 indicated a statistical difference represented by an asterisk.
- (c,g) Multiple comparisons were tested with the Kruskal–Wallis rank sum test followed by Dunn post hoc tests using the Benjamini–Hochberg method for P -values adjustment. Different letters above box plots indicate a statistical difference (P -value < 0.05) between the corresponding genotypes.

or proteins. We found that 82 *NLR* genes, out of the 207 coded in *Arabidopsis*, and two *NLR* proteins (ZAR1 and TN8) were up-regulated in 12-day-old *snap33-1* seedlings, including the *AT3G04220*, *AT4G11170*, and *AT2G32140* *NLR* genes (Data S1, S2, and S3). These observations thus suggested that these *NLR*s could potentially contribute to the phenotype of *snap33* mutants. Some rare R proteins have been reported to signal independently of EDS1 and NDR1, such as the ZAR1 singleton-CNL (Adachi et al., 2019; Lewis et al., 2010). The involvement of such a R protein in guarding SNAP33 could explain the different reversion levels in *snap33-1 ndr1-1 eds1-2* and *snap33-1 35S::NahG* mutants. Interestingly, ZAR1 transcripts and proteins were about 3 and 4 times more abundant, respectively, in *snap33-1* compared to WT (Data S1 and S2). This prompted us to cross *snap33-1* with the *zar1-3* mutant (Lewis et al., 2010). However, we did not observe any reversion effect, suggesting that ZAR1 is not implicated in guarding SNAP33 (Figure S12d–f).

Accumulation of PTI and ETI signaling proteins and MAPK priming in the *snap33-1* mutant is SA-dependent

The RNA-seq and DIA-MS data revealed that the *snap33-1* mutant accumulates key PTI and ETI signaling components at both the transcript and protein levels (Data S1 and S2). For instance, the DIA-MS results showed an increased abundance of several RLKs, MAPKs, and CDPKs (Figure S13a). Interestingly, it was recently reported that *NLR* activation in ETI leads to the accumulation of PTI signaling components, both at the transcript and protein levels (Ngou, Ahn, et al., 2021; Yuan et al., 2021). To further support our transcriptomic and proteomic data, and assess the involvement of SA signaling in the accumulation of these proteins, we carried out immunoblotting analyses with antibodies recognizing several key PTI and ETI proteins. We observed that the SA marker PR1 highly accumulated in *snap33* mutants but was undetectable in *snap33-1 35S::NahG* and the control genotypes (Figure 8a; Figure S13b). The RLP co-receptor SOBIR1, the NADPH oxidase RBOHD, and EDS1 accumulated in *snap33* mutants but this accumulation was reduced in *snap33-1 35S::NahG*. Overall, these results showed that PTI and ETI signaling

proteins accumulate in *snap33* mutants in a partially SA-dependent manner.

The accumulation of PTI signaling components prompted us to evaluate the response of *snap33* mutants to PTI and the involvement of SA signaling in this response. Given the severity of the *snap33* phenotype, we tested the immune MAPK activation upon treatment with the MAMP flg22. We observed that the activation of MPK3, MPK4, and MPK6 was slightly increased in the *snap33-1* mutant but that this activation was WT-like in *snap33-1 sid2-2* (Figure 8b; Figure S13c). This enhanced activation was actually correlated to an increased accumulation of the three MAPK proteins in the *snap33-1* mutant (Figure 8b), further confirming the accumulation of PTI proteins observed above (Figure 8a; Figure S13b). These results thus showed that MAPK signaling is primed in the *snap33-1* mutant and that this priming is SA-dependent.

The above results notably showed the preponderant contribution of SA signaling for the establishment of the macroscopic and molecular *snap33* phenotypes. To better understand this contribution, we measured the SA and SAG contents in *snap33-1 35S::NahG* and *snap33-1 sid2-2*. Compared to WT and *snap33-1*, *snap33-1 35S::NahG* accumulated intermediate amounts of SA, whereas SAG was hardly detectable (Figure 8c). The absence of PR1 protein detection observed above in *snap33-1 35S::NahG* (Figure 8a) suggests however that there is no active SA signaling. Regarding *snap33-1 sid2-2*, the mutant accumulated the same levels of SA and SAG as WT (Figure 8c), suggesting no SA signaling occurs, in agreement with the basal level of *PR1* transcripts observed previously (Figure 5e). The rosette FW difference observed for *snap33-1 35S::NahG* and *snap33-1 sid2-2* (Figure 6b,c) thus suggests that the homeostasis of SA evolves differently during the development of these two genotypes.

As numerous PTI signaling components were up-regulated in both the transcriptome and proteome of the *snap33-1* mutant (Figure S13a, Data S1 and S2), it suggested that a PTI-like response might occur at steady state in the mutant. To examine this hypothesis, although knowing that an ETI-like response simultaneously occurs in this autoimmune mutant, we compared the transcriptome and

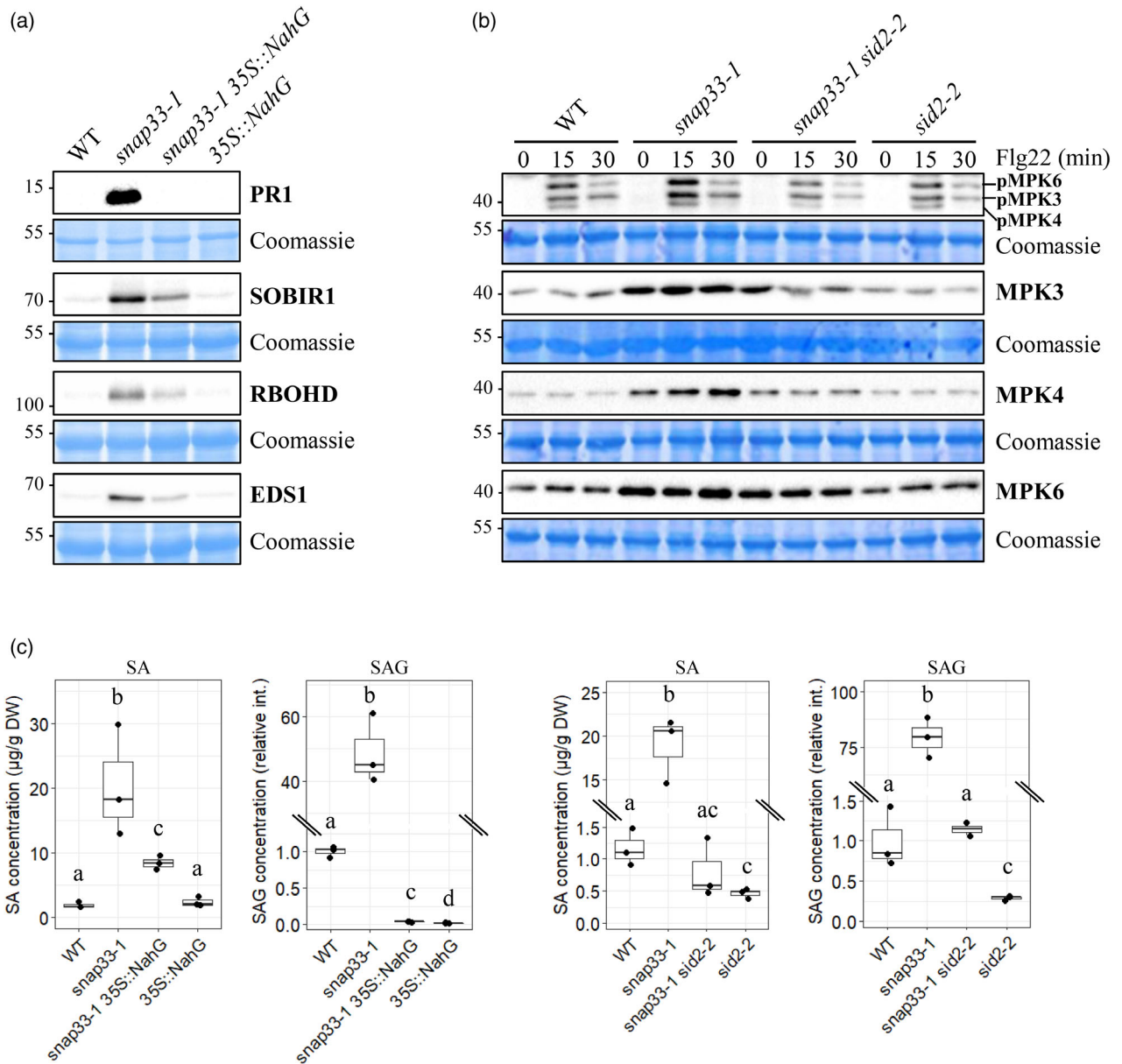


Figure 8. Accumulation of PTI and ETI signaling proteins and MAPK priming in *snap33-1* mutant is SA-dependent. (a) Representative immunoblottings of four independent biological repeats carried out on protein extracts from 13-day-old seedlings. In this study, 10 µg proteins were loaded for the anti-PR1 immunoblottings and 30 µg for the other immunoblottings. (b) Representative immunoblottings of three to four independent biological repeats carried out on protein extracts from 13-day-old seedlings that had been subjected to a 100 nM flg22 treatment kinetics. pMPK_i stands for the activated form of MAPKs as revealed by their phosphorylated state using the anti-phospho-p44/42 MAPK (Erk1/2) (Thr202/Tyr204) monoclonal antibody. (a,b) Coomassie blue stainings (Coomassie) of blots indicate the equal loading of protein samples. Molecular weights are indicated in kDa on the left of blots. (c) Absolute and relative quantification of SA (DW: dry weight) and SAG (int.: intensity), respectively, were carried out by UPLC-MS/MS analyses. Three independent biological repeats were performed. Multiple comparisons were tested with the non-parametric two-sided Tukey test with a confidence level set to 95% using the nparcomp package in R. Different letters above box plots indicate a statistical difference (P-value < 0.05) between the corresponding genotypes.

proteome of the *snap33-1* mutant to reported PTI-induced transcriptome and proteome changes, respectively (Bassal et al., 2020; Bjornson et al., 2021). In this study, 76.3% (740 out of 970) and 67.7% (63 out of 93) of genes commonly up- and down-regulated by seven different elicitors, respectively, were similarly up- and down-regulated in

snap33-1 mutant (Figure S14a and Data S4). In addition, 42.1% (188 out of 447) and 24.3% (41 out of 169) of proteins up- and down-regulated in the *snap33-1* mutant were similarly identified as up- and down-regulated upon flg22 treatment, respectively (Figure S14b and Data S5). Given the different experimental setups and the technical

limitations of proteomic approaches, we considered that these different overlaps were highly significant, supporting constitutive PTI-like signaling in the *snap33-1* mutant.

DISCUSSION

snap33 is an autoimmune mutant

We isolated *snap33* knock-out mutants in Col-0 ecotype (Figure 1a; Figure S1a). Their macroscopic phenotypes were similar to the one previously reported in Ws ecotype (*snap33^{Ws}*), suggesting that the genetic determinants responsible for their dwarfism and necrotic lesions are conserved in both ecotypes (Figure 1b). The few reported elements of *snap33* phenotype were reminiscent of autoimmunity (Heese et al., 2001). We established that *snap33* is indeed an autoimmune mutant, exhibiting constitutive cell death, H₂O₂ and SA accumulation, and up-regulation of defense-related transcripts and proteins (Figures 1c, 4a, b, and 8a). Interestingly, the down-regulation of StSNAP33 from potato *Solanum tuberosum* leads to a similar phenotype, including the development of necrotic regions and SA accumulation, suggesting that the molecular determinants responsible for the *snap33* phenotype are sufficiently conserved in these relatively distant species (Eschen-Lippold et al., 2012). In the light of our results, we suggest that down-regulation of StSNAP33 may similarly lead to NLR signaling in potato.

Massive transcriptional and translational reprogramming occurs in the *snap33* mutant

RNA-seq analyses of the *snap33* mutant revealed major changes compared to WT plants. In this study, 7998 DEGs were indeed identified in 12-day-old *snap33* seedlings (Figure 2c,d and Data S1). Importantly, 5-day-old *snap33* seedlings already displayed 2591 DEGs (Figure 2b,d and Data S1), meaning that molecular deregulations appear early, while macroscopic phenotypes still have not arisen. SNAP33 forms SNARE complexes with the Qa-SNARE/syntaxin SYP121/PEN1 and the VAMP721 and VAMP722 R-SNAREs (Kwon et al., 2008). The *syp121 syp122* double mutant exhibits a phenotype similar to the *snap33* mutant, although spontaneous lesions appear later, after 2–3 weeks of growth (Zhang et al., 2007). Interestingly, the transcriptome of *syp121 syp122* was reported (Zhang et al., 2008), and comparison to our data revealed that 93.6% of the 357 up-regulated genes in 2.5-week-old *syp121 syp122* seedlings were also up-regulated in 12-day-old *snap33* mutant seedlings, suggesting the probable involvement of similar signaling mechanisms in both mutants (Figure S15 and Data S6).

We also carried out a large-scale quantitative proteomic analysis which revealed that several hundred proteins differentially accumulate in the *snap33* mutant, with 447 up-regulated and 169 down-regulated proteins showing at

least a 1.5-fold change (Figure 3a,b and Data S2). Interestingly, numerous proteins with unknown or unclear function highly accumulate in *snap33*, which suggests their probable involvement in immune processes.

SA is the main phytohormone contributing to the *snap33* phenotype

The RNA-seq and DIA-MS data notably revealed the enrichment of defense hormone-related processes in the *snap33-1* mutant. The measurement of SA, SAG, JA and ET contents in *snap33* mutants as well as the expression measurement of key marker genes of these defense hormones confirmed their accumulation and active signaling (Figure 4a,b). Our systematic genetic analysis underlined the preponderant role of SA with a synergistic effect of JA (Figure 5). Of note, the SA-JA antagonism is often documented, but synergistic effects were also reported, such as their joint contribution to the RPS2 CNL-mediated ETI (Liu et al., 2016; Tsuda et al., 2009). Our work highlighted the constitutive SAR signaling in *snap33*, which we genetically confirmed by showing the additive/synergistic effect of SA and NHP (Figure 5g,h). This additive/synergistic effect observed in *snap33* autoimmune mutant is in agreement with the mutual amplification loop that SA and NHP establish during pathogen response to promote SAR (Peng et al., 2021). As SA can be produced by both the IC and PAL pathways, we also genetically investigated the contribution of these pathways by comparing the effects of *sid2-2* and *pbs3-2* mutations, as well as the ectopic expression of NahG. The slight and similar effects of *sid2-2* and *pbs3-2* mutations compared to the strong effect of NahG expression suggested that in *snap33-1* both the IC and PAL pathways strongly contribute to SA signaling (Figure 6b,c). Moreover, we showed that mutation of the key SA receptor *NPR1* only slightly suppressed the *snap33-1* phenotype (Figure 6d,e), suggesting the involvement of other SA receptors such as NPR3/NPR4 as their roles in SA signaling was previously established during both PTI and ETI (Liu et al., 2020). We cannot rule out the possibility that other SA-binding proteins (SABPs) may also be involved. Many SABPs were indeed identified, but their contributions to SA-mediated immunity are still unclear (Klessig et al., 2016; Peng et al., 2021).

NLR signaling contributes to the *snap33* phenotype

Given the autoimmune phenotype of the *snap33* mutant and the strong suppression observed by expressing NahG, we favored the hypothesis that SNAP33 would be guarded by NLR(s). We found that *ndr1-1* and *eds1-2* mutations slightly suppressed the *snap33-1* phenotype, and observed an additive/synergistic effect with their simultaneous mutations (Figure 7b,c). These results could suggest that SNAP33 would be guarded by at least one sensor NLR, of CNL type, but also that *NDR1*- and *EDS1*-independent R

signaling would be involved. Some R proteins are believed to be independent of NDR1 and EDS1, such as the CNLs ZAR1 and RPP13 (Bittner-Eddy & Beynon, 2001; Lewis et al., 2010). Moreover, resistance conferred by the CNLs RPP7 and RPP8 is only slightly suppressed by *ndr1-1 eds1-2* double mutant (McDowell et al., 2000). Alternatively, our results may suggest that SNAP33 would be guarded by one or several of these atypical NLRs, leading to SA signaling and then notably to SA-dependent accumulation of typical NLRs which would signal through EDS1 and NDR1. Among these atypical CNLs, ZAR1 transcript and protein levels were up-regulated in *snap33-1*. We thus examined the effect of the *zar1-3* mutation but did not observe any reversion of the *snap33-1* phenotype (Figure S12d,e). We conclude that ZAR1 does not guard SNAP33, although there is still the possibility that an additional atypical NLR guards SNAP33 or that an *NDR1*- and *EDS1*-dependent signaling is triggered, which would prevent to observe any ZAR1 effect. To test this second hypothesis, one would need to generate a *snap33-1 ndr1-1 eds1-2 zar1-3* quadruple mutant. Besides, AMSH3 activity is necessary for immunity mediated by the CNLs RPM1 and RPS2 (Schultz-Larsen et al., 2018). As we observed a slight suppressive effect of *amsh3-4* on the *snap33-1* mutant phenotype (Figure 7f,g), these CNLs could also be implicated.

Mutants of SNAP33 protein partners also exhibit dwarfism and necrotic leaf lesions, although their symptoms seem to appear later and be less severe. Indeed, the *syp121 syp122* double mutant and RNAi-silenced lines in which both *VAMP721* and *VAMP722* transcript levels are strongly reduced, grow normally for 2–3 weeks before necrotic lesions appear and plants display a stunted growth (Kwon et al., 2008; Zhang et al., 2007). Regarding the *exo70b1* mutant, it develops spontaneous lesions after 5 weeks of growth (Zhao et al., 2015). The *syp121 syp122* phenotype was reported to be partially reverted by *amsh3* mutations (Schultz-Larsen et al., 2018). We found that the *amsh3-4* mutation led to a seemingly weaker suppression of the *snap33-1* phenotype (Figure 7f,g). Likewise, whereas the *tn2-1* mutation was shown to clearly suppress the *exo70b1* phenotype, *tn2-1* alone had no effect on the *snap33-1* phenotype (Figure 7f,g) (Zhao et al., 2015). These results support the above observations that the *snap33* phenotype is more severe than those of the mutants of its protein partners.

Our results indicate that constitutive R signaling occurs in the *snap33* mutant but do not clearly establish whether SNAP33 protein itself or its function is guarded. It is actually interesting to note that *Nicotiana benthamiana* SNAP33 might interact with the PexRD12 effector from the potato blight pathogen *Phytophthora infestans*, as was reported from co-immunoprecipitation analyses, although this interaction deserves further investigations (Petre et al., 2021). Besides, EXO70B1 was shown to be the direct

target of *Pseudomonas syringae* AvrPtoB and *Xanthomonas campestris* XopP effectors (Michalopoulou et al., 2022; Wang et al., 2019). AvrPtoB is an E3 ligase that ubiquitinates EXO70B1 thus leading to its degradation via the 26S proteasome, and XopP binds EXO70B1 and hence blocks exocyst-dependent exocytosis.

Accumulation of PTI proteins in the *snap33-1* mutant is SA-dependent

We observed in the RNA-seq and DIA-MS data that the *snap33-1* mutant accumulated PTI signaling components. It was recently reported that ETI activated by TNLs or CNLs leads to the accumulation of PTI signaling components (Ngou, Ahn, et al., 2021; Yuan et al., 2021). It was thus not so surprising to observe the same in a mutant exhibiting constitutive ETI-like responses. However, we additionally showed that this accumulation at the protein level was only partly SA-dependent (Figure 8a). Interestingly, a report showed that transcripts of several PTI (e.g., PRRs, MAPKs, and CDPKs) and ETI (e.g., EDS1, NDR1, and ZAR1) signaling components accumulate in response to a 1 h SA treatment (Ding et al., 2018). It would thus be interesting to verify that this accumulation of PTI components is likewise SA-dependent in classical NLR-triggered ETI responses, and, besides SA signaling, decipher the mechanism, of how ETI responses and accumulation of PTI components are linked.

EXPERIMENTAL PROCEDURES

Plant materials and growth conditions

Full descriptions of generated and used plant lines, as well as their growth conditions, are shown in Methods S1 and Table S1.

Trypan blue and DAB stainings

Trypan blue and 3,3'-diaminobenzidine (DAB) stainings were carried out on 21-day-old seedlings. Three independent biological repeats were performed. Details are included in Methods S2.

RNA-sequencing analyses

Three independent biological replicates of 5-day-old and 12-day-old WT-1 and *snap33-1* mutant seedlings were produced. RNA-seq libraries were constructed from total RNA by the POPS platform (IPS2). Differential expression analysis was performed using the Bioconductor package edgeR (v 3.26.8). The differential analysis was based on a negative binomial generalized log-linear model (GLM). Genes with an adjusted *P*-value (FDR, Benjamini–Hochberg adjustment [Benjamini & Hochberg, 1995]) below 0.05 were considered as differentially expressed genes (DEGs). A full description is presented in Methods S3.

DIA-MS analyses

Three independent biological replicates of 12-day-old WT-1 and *snap33-1* mutant seedlings were produced. Total proteins were digested and further prepared for data-independent acquisition mass spectrometry (DIA-MS) analysis. Data were analyzed using Spectronaut software (v 14) to identify and quantify peptides and

proteins. A paired Student's *t* test, based on the log₂ ratios of the peptide intensities of the individual peptides of a protein, was performed to uncover differential expression between samples. Resulting *P*-values were corrected for multiple testing using the *q*-value approach to control the overall FDR. Proteins with a *q*-value <0.01 were considered as differentially expressed proteins (DEPs). Details are included in Methods S4.

qRT-PCR experiments

For quantitative reverse transcription-PCR (qRT-PCR) analyses, three independent biological repeats were performed. Differences were tested with the non-parametric Wilcoxon rank sum test, and *P*-value <0.05 indicated a statistical difference. A full description is presented in Methods S5 and used primers are listed in Table S2.

Phytohormone measurements

Quantifications of salicylic acid (SA), SA O-glucoside (SAG) and jasmonic acid (JA) were performed by UPLC-MS/MS analyses, and ethylene (ET) measurements were carried out as described by Thain *et al.* (Thain *et al.*, 2004). At least three independent biological repeats were performed. Two-sample differences were tested with the non-parametric Wilcoxon rank sum test, and *P*-value <0.05 indicated a statistical difference. Multiple (>2) comparisons were tested with the non-parametric two-sided Tukey test with a confidence level set to 95% using the nparcomp package in R (Konietschke *et al.*, 2015). Detailed descriptions are shown in Methods S6.

Rosette fresh weight measurements

Plant rosettes were cut and individually weighed. Due to the severe effect of the *snap33-1* mutation on phenotypes, genotypes containing the *snap33-1* mutation were compared together, and control genotypes were compared together separately. Multiple (>2) comparisons were tested with the non-parametric Kruskal-Wallis rank sum test followed by Dunn post hoc tests using the Benjamini-Hochberg method for *P*-values adjustment, and *P*-value <0.05 indicated a statistical difference. Details are presented in Methods S7.

Gene ontology analyses

Gene ontology (GO) analyses were performed as described by Alexa *et al.* (Alexa *et al.*, 2006).

Immunoblotting assays

Protein extracts from 13-day-old seedlings were subjected to immunoblotting assays using various primary antibodies. Three to four independent biological replicates were performed. Details are included in Methods S8.

ACCESSION NUMBERS

Accession numbers of genes experimentally associated with this work are listed in Table S3.

ACKNOWLEDGEMENTS

We are grateful to the following people for sharing materials: Livia Merendino (*ein2-1*), Cécile Raynaud (*35S::NahG*), Graham Noctor (*npr1-1*), Marie Boudsocq (*cpk5-1*), Dingzhong Tang (*tn2-1*), and Hans Thordal-Christensen (*amsh3-4*). We thank Gwilherm Brisou for help with ethylene measurement, and Gabrièle Adam for help with some R scripts. We thank Farid El Kasmi and members of the

Stress Signaling group of IPS2 for the critical discussion of this work.

FUNDING INFORMATION

This work has benefited from a doctoral grant to HHe (Ministère de l'enseignement supérieur, de la recherche et de l'innovation—MESRI). The IPS2, POPS platform and IJPB benefit from the support of the EUR Saclay Plant Sciences-SPS (ANR-17-EUR-0007).

AUTHOR CONTRIBUTIONS

JB, through insightful discussions with BS, JCo, and HHi, designed the work. HHe, JB, NR, HA, JCa, CPLR, and SC performed the experiments, and HHe and JB analyzed the data. JB wrote the manuscript with contributions from all authors.

CONFLICT OF INTEREST STATEMENT

The authors declare no conflict of interest.

DATA AVAILABILITY STATEMENT

RNA-seq data were deposited at Gene Expression Omnibus (Edgar *et al.*, 2002): <http://www.ncbi.nlm.nih.gov/geo/>; accession number GSE247242. All steps of the experiment, from growth conditions to bioinformatic analyses, were detailed in CATdb (Gagnot *et al.*, 2008): <https://catdb.ips2.universite-paris-saclay.fr/>; project number NGS2021_03_Snap33, according to the MINSEQE 'minimum information about a high-throughput sequencing experiment'. DIA-MS data were deposited at the ProteomeXchange Consortium via the PRIDE partner repository with the identifier PXD046860. Genetic materials presented in this work are available upon request to the corresponding author Jean Bigeard.

SUPPORTING INFORMATION

Additional Supporting Information may be found in the online version of this article.

Data S1. RNA-seq results.

Data S2. DIA-MS results.

Data S3. NLR genes found up-regulated in the *snap33-1* RNA-seq data.

Data S4. Comparison of the *snap33-1* RNA-seq data to the report by Bjornson *et al.*, 2021.

Data S5. Comparison of the *snap33-1* DIA-MS data to the report by Bassal *et al.*, 2020.

Data S6. Comparison of the *snap33-1* RNA-seq data to the report by Zhang *et al.*, 2008.

Figure S1. Isolation and characterization of new *snap33* T-DNA mutants.

Figure S2. Experimental design of *snap33-1* and WT-1 growth and harvest for RNA-seq analyses.

Figure S3. GO enrichment analyses of biological processes among the DEGs up-regulated in *snap33-1* at 5 and 12 days.

Figure S4. Overlap between the 'plant-type hypersensitive response' GO category and genes up-regulated in *snap33-1* at 12 days.

Figure S5. GO enrichment analyses of biological processes among the DEGs down-regulated in *snap33-1* at 5 and 12 days.

Figure S6. Heatmap showing the clustering of the six samples (2 genotypes x 3 biological repeats) analyzed by DIA-MS.

Figure S7. GO enrichment analyses of biological processes among the 169 DEPs down-regulated in *snap33-1*.

Figure S8. Heatmap showing the clustering of the 247 DEGs/DEPs from the sets of DEGs with $|\log_2FC| \geq 1$ (P -value < 0.05) and DEPs with $|\log_2FC| \geq 0.58$ (q -value < 0.01).

Figure S9. Heatmap showing DEPs related to phytohormone synthesis.

Figure S10. Rosette FW measurement of 35-day-old plants in the context of phytohormonal contribution to *snap33-1* mutant phenotype.

Figure S11. Rosette FW measurement of 35-day-old plants in the context of SA synthesis/perception contribution to *snap33-1* mutant phenotype.

Figure S12. Rosette FW measurement of 35-day-old plants in the context of NLR signaling contribution to *snap33-1* mutant phenotype.

Figure S13. Accumulation of PTI and ETI signaling proteins and MAPK priming in *snap33* mutants.

Figure S14. Comparison of the transcriptome and proteome of *snap33-1* mutant to reported PTI-induced transcriptome and proteome changes.

Figure S15. Comparison of the up-regulated DEGs in *snap33-1* mutant versus reported up-regulated DEGs in *syp121 syp122* double mutant.

Methods S1. Plant materials and growth conditions.

Methods S2. Trypan blue and DAB stainings.

Methods S3. RNA-sequencing analyses.

Methods S4. DIA-MS analyses.

Methods S5. qRT-PCR experiments.

Methods S6. Phytohormone measurements.

Methods S7. Rosette fresh weight measurements.

Methods S8. Immunoblotting assays.

Table S1. List of all the Arabidopsis lines used and generated in this work.

Table S2. List of all the primers used in this work.

Table S3. List of accession numbers (AGIs) of genes experimentally associated with the present work.

REFERENCES

- Acosta, I.F., Gasperini, D., Chételat, A., Stolz, S., Santuari, L. & Farmer, E.E. (2013) Role of NINJA in root jasmonate signaling. *Proceedings of the National Academy of Sciences of the United States of America*, **110**, 15473–15478.
- Adachi, H., Derevnina, L. & Kamoun, S. (2019) NLR singletons, pairs, and networks: evolution, assembly, and regulation of the intracellular immunoreceptor circuitry of plants. *Current Opinion in Plant Biology*, **50**, 121–131.
- Aerts, N., Pereira Mendes, M. & Van Wees, S.C.M. (2021) Multiple levels of crosstalk in hormone networks regulating plant defense. *The Plant Journal*, **105**, 489–504.
- Alexa, A., Rahnenführer, J. & Lengauer, T. (2006) Improved scoring of functional groups from gene expression data by decorrelating GO graph structure. *Bioinformatics*, **22**, 1600–1607.
- Alonso, J.M., Hirayama, T., Roman, G., Nourizadeh, S. & Ecker, J.R. (1999) EIN2, a bifunctional transducer of ethylene and stress responses in *Arabidopsis*. *Science*, **284**, 2148–2152.
- Altmann, M., Altmann, S., Rodriguez, P.A., Weller, B., Elorduy Vergara, L., Palme, J. et al. (2020) Extensive signal integration by the phytohormone protein network. *Nature*, **583**, 271–276.
- Bartsch, M., Gobbato, E., Bednarek, P., Debey, S., Schultze, J.L., Bautor, J. et al. (2006) Salicylic acid-independent ENHANCED DISEASE SUSCEPTIBILITY1 signaling in Arabidopsis immunity and cell death is regulated by the monooxygenase FMO1 and the Nudix hydrolase NUDT7. *Plant Cell*, **18**, 1038–1051.
- Bassal, M., Abukhalaf, M., Majovsky, P., Thieme, D., Herr, T., Ayash, M. et al. (2020) Reshaping of the *Arabidopsis thaliana* proteome landscape and Co-regulation of proteins in development and immunity. *Molecular Plant*, **13**, 1709–1732.
- Benjamini, Y. & Hochberg, Y. (1995) Controlling the false discovery rate: a practical and powerful approach to multiple testing. *Journal of the Royal Statistical Society, Series B*, **57**, 289–300.
- Bhandari, D.D., Lapin, D., Kracher, B., von Born, P., Bautor, J., Niefind, K. et al. (2019) An EDS1 heterodimer signalling surface enforces timely reprogramming of immunity genes in *Arabidopsis*. *Nature Communications*, **10**, 772.
- Bigeard, J., Colcombet, J. & Hirt, H. (2015) Signaling mechanisms in pattern-triggered immunity (PTI). *Molecular Plant*, **8**, 521–539.
- Bittner-Eddy, P.D. & Beynon, J.L. (2001) The Arabidopsis downy mildew resistance gene, RPP13-Nd, functions independently of NDR1 and EDS1 and does not require the accumulation of salicylic acid. *Molecular Plant-Microbe Interactions*, **14**, 416–421.
- Bjornson, M., Pimprikar, P., Nürnberger, T. & Zipfel, C. (2021) The transcriptional landscape of *Arabidopsis thaliana* pattern-triggered immunity. *Nature Plants*, **7**, 579–586.
- Boudsocq, M., Willmann, M.R., McCormack, M., Lee, H., Shan, L., He, P. et al. (2010) Differential innate immune signalling via Ca²⁺ sensor protein kinases. *Nature*, **464**, 418–422.
- Bruggeman, Q., Raynaud, C., Benhamed, M. & Delarue, M. (2015) To die or not to die? Lessons from lesion mimic mutants. *Frontiers in Plant Science*, **6**, 24.
- Cao, H., Glazebrook, J., Clarke, J.D., Volko, S. & Dong, X. (1997) The Arabidopsis NPR1 gene that controls systemic acquired resistance encodes a novel protein containing ankyrin repeats. *Cell*, **88**, 57–63.
- Century, K.S., Shapiro, A.D., Repetti, P.P., Dahlbeck, D., Holub, E. & Staskawicz, B.J. (1997) NDR1, a pathogen-induced component required for Arabidopsis disease resistance. *Science*, **278**, 1963–1965.
- Chen, Y.-C., Holmes, E.C., Rajniak, J., Kim, J.-G., Tang, S., Fischer, C.R. et al. (2018) N-hydroxy-pipecolic acid is a mobile metabolite that induces systemic disease resistance in *Arabidopsis*. *Proceedings of the National Academy of Sciences of the United States of America*, **115**, E4920–E4929.
- Dewdney, J., Reuber, T.L., Wildermuth, M.C., Devoto, A., Cui, J., Stutius, L.M. et al. (2000) Three unique mutants of *Arabidopsis* identify eds loci required for limiting growth of a biotrophic fungal pathogen. *The Plant Journal*, **24**, 205–218.
- Ding, P. & Ding, Y. (2020) Stories of salicylic acid: a plant defense hormone. *Trends in Plant Science*, **25**, 549–565.
- Ding, Y., Sun, T., Ao, K., Peng, Y., Zhang, Y., Li, X. et al. (2018) Opposite roles of salicylic acid receptors NPR1 and NPR3/NPR4 in transcriptional regulation of plant immunity. *Cell*, **173**, 1454–1467.e15.
- Edgar, R., Domrachev, M. & Lash, A.E. (2002) Gene expression omnibus: NCBI gene expression and hybridization array data repository. *Nucleic Acids Research*, **30**, 207–210.
- El Kasmi, F., Krause, C., Hiller, U., Stierhof, Y.-D., Mayer, U., Conner, L. et al. (2013) SNARE complexes of different composition jointly mediate membrane fusion in *Arabidopsis* cytokinesis. *Molecular Biology of the Cell*, **24**, 1593–1601.
- Eschen-Lippold, L., Landgraf, R., Smolka, U., Schulze, S., Heilmann, M., Heilmann, I. et al. (2012) Activation of defense against Phytophthora infestans in potato by down-regulation of syntaxin gene expression. *The New Phytologist*, **193**, 985–996.
- Gagnot, S., Tamby, J.-P., Martin-Magniette, M.-L., Bitton, F., Taconnat, L., Balzergue, S. et al. (2008) CATdb: a public access to *Arabidopsis* transcriptome data from the URGV-CATMA platform. *Nucleic Acids Research*, **36**, D986–D990.
- Gu, X., Brennan, A., Wei, W., Guo, G. & Lindsey, K. (2020) Vesicle transport in plants: a revised phylogeny of SNARE proteins. *Evolutionary Bioinformatics Online*, **16**, 1176934320956575.
- Gu, Y., Zavaliev, R. & Dong, X. (2017) Membrane trafficking in plant immunity. *Molecular Plant*, **10**, 1026–1034.

- Guzmán, P. & Ecker, J.R. (1990) Exploiting the triple response of *Arabidopsis* to identify ethylene-related mutants. *Plant Cell*, **2**, 513–523.
- Hartmann, M., Zeier, T., Bernsdorff, F., Reichel-Deland, V., Kim, D., Hohmann, M. *et al.* (2018) Flavin monooxygenase-generated N-Hydroxy-pipecolic acid is a critical element of plant systemic immunity. *Cell*, **173**, 456–469.e16.
- Heese, M., Gansel, X., Sticher, L., Wick, P., Grebe, M., Granier, F. *et al.* (2001) Functional characterization of the KNOLLE-interacting t-SNARE AtSNAP33 and its role in plant cytokinesis. *The Journal of Cell Biology*, **155**, 239–249.
- Jones, J.D. & Dangl, J.L. (2006) The plant immune system. *Nature*, **444**, 323–329.
- Kapos, P., Devendrakumar, K.T. & Li, X. (2019) Plant NLRs: from discovery to application. *Plant Science*, **279**, 3–18.
- Klessig, D.F., Tian, M. & Choi, H.W. (2016) Multiple targets of salicylic acid and its derivatives in plants and animals. *Frontiers in Immunology*, **7**, 206.
- Konietzschke, F., Placzek, M., Schaarschmidt, F. & Hothorn, L.A. (2015) Nparcomp: an R software package for nonparametric multiple comparisons and simultaneous confidence intervals. *Journal of Statistical Software*, **64**, 1–17.
- Kwon, C., Neu, C., Pajonk, S., Yun, H.S., Lipka, U., Humphry, M. *et al.* (2008) Co-option of a default secretory pathway for plant immune responses. *Nature*, **451**, 835–840.
- Lang, J., Genot, B., Bigeard, J. & Colcombet, J. (2022) MPK3 and MPK6 control salicylic acid signaling by up-regulating NLR receptors during pattern- and effector-triggered immunity. *Journal of Experimental Botany*, **73**, 2190–2205.
- Lapin, D., Bhandari, D.D. & Parker, J.E. (2020) Origins and immunity networking functions of EDS1 family proteins. *Annual Review of Phytopathology*, **58**, 253–276.
- Lawton, K., Weymann, K., Friedrich, L., Vernooij, B., Uknes, S. & Ryals, J. (1995) Systemic acquired resistance in *Arabidopsis* requires salicylic acid but not ethylene. *Molecular Plant-Microbe Interactions*, **8**, 863–870.
- Lewis, J.D., Wu, R., Guttman, D.S. & Desveaux, D. (2010) Allele-specific virulence attenuation of the *Pseudomonas syringae* HopZ1a type III effector via the *Arabidopsis* ZAR1 resistance protein. *PLoS Genetics*, **6**, e1000894.
- Lipka, V., Kwon, C. & Panstruga, R. (2007) SNARE-ware: the role of SNARE-domain proteins in plant biology. *Annual Review of Cell and Developmental Biology*, **23**, 147–174.
- Liu, L., Sonbol, F.-M., Huot, B., Gu, Y., Withers, J., Mwimba, M. *et al.* (2016) Salicylic acid receptors activate jasmonic acid signalling through a non-canonical pathway to promote effector-triggered immunity. *Nature Communications*, **7**, 13099.
- Liu, N., Hake, K., Wang, W., Zhao, T., Romeis, T. & Tang, D. (2017) CALCIUM-DEPENDENT PROTEIN KINASE5 associates with the truncated NLR protein TIR-NBS2 to contribute to exo70B1-mediated immunity. *Plant Cell*, **29**, 746–759.
- Liu, Y., Sun, T., Sun, Y., Zhang, Y., Radojčić, A., Ding, Y. *et al.* (2020) Diverse roles of the salicylic acid receptors NPR1 and NPR3/NPR4 in plant immunity. *Plant Cell*, **32**, 4002–4016.
- Lu, Y. & Tsuda, K. (2021) Intimate association of PRR- and NLR-mediated signaling in plant immunity. *Molecular Plant-Microbe Interactions*, **34**, 3–14.
- McDowell, J.M., Cuzick, A., Can, C., Beynon, J., Dangl, J.L. & Holub, E.B. (2000) Downy mildew (*Peronospora parasitica*) resistance genes in *Arabidopsis* vary in functional requirements for NDR1, EDS1, NPR1 and salicylic acid accumulation. *The Plant Journal*, **22**, 523–529.
- Mergner, J., Frejno, M., List, M., Papacek, M., Chen, X., Chaudhary, A. *et al.* (2020) Mass-spectrometry-based draft of the *Arabidopsis* proteome. *Nature*, **579**, 409–414.
- Meyer, D., Pajonk, S., Micali, C., O'Connell, R. & Schulze-Lefert, P. (2009) Extracellular transport and integration of plant secretory proteins into pathogen-induced cell wall compartments. *The Plant Journal*, **57**, 986–999.
- Michalopoulou, V.A., Mermigka, G., Kotsaridis, K., Mentzelopoulou, A., Celie, P.H.N., Moschou, P.N. *et al.* (2022) The host exocyst complex is targeted by a conserved bacterial type-III effector that promotes virulence. *Plant Cell*, **34**, 3400–3424.
- Nawrath, C. & Métraux, J.P. (1999) Salicylic acid induction-deficient mutants of *Arabidopsis* express PR-2 and PR-5 and accumulate high levels of camalexin after pathogen inoculation. *Plant Cell*, **11**, 1393–1404.
- Ngou, B.P.M., Ahn, H.-K., Ding, P. & Jones, J.D.G. (2021) Mutual potentiation of plant immunity by cell-surface and intracellular receptors. *Nature*, **592**, 110–115.
- Ngou, B.P.M., Ding, P. & Jones, J.D.G. (2022) Thirty years of resistance: zig-zag through the plant immune system. *Plant Cell*, **34**, 1447–1478.
- Ngou, B.P.M., Jones, J.D.G. & Ding, P. (2021) Plant immune networks. *Trends in Plant Science*, **27**, 255–273. Available from: <https://doi.org/10.1016/j.tplants.2021.08.012>
- Nobuta, K., Okrent, R.A., Stoutemyer, M., Rodibaugh, N., Kempema, L., Wildermuth, M.C. *et al.* (2007) The GH3 acyl adenylase family member PBS3 regulates salicylic acid-dependent defense responses in *Arabidopsis*. *Plant Physiology*, **144**, 1144–1156.
- Pecenková, T., Hála, M., Kulich, I., Kocourková, D., Drdová, E., Fendrych, M. *et al.* (2011) The role for the exocyst complex subunits Exo70B2 and Exo70H1 in the plant-pathogen interaction. *Journal of Experimental Botany*, **62**, 2107–2116.
- Peng, Y., Yang, J., Li, X. & Zhang, Y. (2021) Salicylic acid: biosynthesis and signaling. *Annual Review of Plant Biology*, **72**, 761–791.
- Petre, B., Contreras, M.P., Bozkurt, T.O., Schattat, M.H., Sklenar, J., Schornack, S. *et al.* (2021) Host-interactor screens of *Phytophthora infestans* RXLR proteins reveal vesicle trafficking as a major effector-targeted process. *Plant Cell*, **33**, 1447–1471.
- Pruitt, R.N., Locci, F., Wanke, F., Zhang, L., Saile, S.C., Joe, A. *et al.* (2021) The EDS1-PAD4-ADR1 node mediates *Arabidopsis* pattern-triggered immunity. *Nature*, **598**, 495–499.
- Rodríguez, E., El Ghouli, H., Mundy, J. & Petersen, M. (2016) Making sense of plant autoimmunity and “negative regulators”. *The FEBS Journal*, **283**, 1385–1391.
- Saur, I.M.L., Panstruga, R. & Schulze-Lefert, P. (2021) NOD-like receptor-mediated plant immunity: from structure to cell death. *Nature Reviews. Immunology*, **21**, 305–318.
- Schultz-Larsen, T., Lenk, A., Kalinowska, K., Vestergaard, L.K., Pedersen, C., Isono, E. *et al.* (2018) The AMSH3 ESCRT-III-associated Deubiquitinase is essential for plant immunity. *Cell Reports*, **25**, 2329–2338.e5.
- Thain, S.C., Vandenbussche, F., Laarhoven, L.J.J., Dowson-Day, M.J., Wang, Z.-Y., Tobin, E.M. *et al.* (2004) Circadian rhythms of ethylene emission in *Arabidopsis*. *Plant Physiology*, **136**, 3751–3761.
- Tian, H., Wu, Z., Chen, S., Ao, K., Huang, W., Yaghmaiean, H. *et al.* (2021) Activation of TIR signalling boosts pattern-triggered immunity. *Nature*, **598**, 500–503.
- Toruño, T.Y., Stergiopoulos, I. & Coaker, G. (2016) Plant-pathogen effectors: cellular probes interfering with plant defenses in spatial and temporal manners. *Annual Review of Phytopathology*, **54**, 419–441.
- Tsuda, K., Sato, M., Stoddard, T., Glazebrook, J. & Katagiri, F. (2009) Network properties of robust immunity in plants. *PLoS Genetics*, **5**, e1000772.
- van Wersich, R., Li, X. & Zhang, Y. (2016) Mighty dwarfs: *Arabidopsis* autoimmune mutants and their usages in genetic dissection of plant immunity. *Frontiers in Plant Science*, **7**, 1717.
- Venugopal, S.C., Jeong, R.-D., Mandal, M.K., Zhu, S., Chandra-Shekhara, A.C., Xia, Y. *et al.* (2009) Enhanced disease susceptibility 1 and salicylic acid act redundantly to regulate resistance gene-mediated signaling. *PLoS Genetics*, **5**, e1000545.
- Vlot, A.C., Sales, J.H., Lenk, M., Bauer, K., Brambilla, A., Sommer, A. *et al.* (2021) Systemic propagation of immunity in plants. *The New Phytologist*, **229**, 1234–1250.
- Wang, W., Liu, N., Gao, C., Rui, L., Jiang, Q., Chen, S. *et al.* (2021) The truncated TNL receptor TN2-mediated immune responses require ADR1 function. *The Plant Journal*, **108**, 672–689. Available from: <https://doi.org/10.1111/tj.15463>
- Wang, W., Liu, N., Gao, C., Rui, L. & Tang, D. (2019) The *Pseudomonas syringae* effector AvrPtoB associates with and ubiquitinates *Arabidopsis* exocyst subunit EXO70B1. *Frontiers in Plant Science*, **10**, 1027.
- Wick, P., Gansel, X., Oulevey, C., Page, V., Studer, I., Dürst, M. *et al.* (2003) The expression of the t-SNARE AtSNAP33 is induced by pathogens and mechanical stimulation. *Plant Physiology*, **132**, 343–351. Available from: <https://doi.org/10.1104/PP.102.012633>
- Wildermuth, M.C., Dewdney, J., Wu, G. & Ausubel, F.M. (2001) Isochorismate synthase is required to synthesize salicylic acid for plant defence. *Nature*, **414**, 562–565.
- Yuan, M., Jiang, Z., Bi, G., Nomura, K., Liu, M., Wang, Y. *et al.* (2021) Pattern-recognition receptors are required for NLR-mediated plant immunity. *Nature*, **592**, 105–109.

- Zárský, V., Kulich, I., Fendrych, M. & Pečenková, T. (2013) Exocyst complexes multiple functions in plant cells secretory pathways. *Current Opinion in Plant Biology*, **16**, 726–733.
- Zeier, J. (2021) Metabolic regulation of systemic acquired resistance. *Current Opinion in Plant Biology*, **62**, 102050.
- Zhang, H., Liu, P., Guo, T., Zhao, H., Bensaddek, D., Aebersold, R. *et al.* (2019) Arabidopsis proteome and the mass spectral assay library. *Scientific Data*, **6**, 278.
- Zhang, Z., Feechan, A., Pedersen, C., Newman, M.-A., Qiu, J., Olesen, K.L. *et al.* (2007) A SNARE-protein has opposing functions in penetration resistance and defence signalling pathways. *The Plant Journal*, **49**, 302–312.
- Zhang, Z., Lenk, A., Andersson, M.X., Gjetting, T., Pedersen, C., Nielsen, M.E. *et al.* (2008) A lesion-mimic syntaxin double mutant in *Arabidopsis* reveals novel complexity of pathogen defense signaling. *Molecular Plant*, **1**, 510–527.
- Zhao, T., Rui, L., Li, J., Nishimura, M.T., Vogel, J.P., Liu, N. *et al.* (2015) A truncated NLR protein, TIR-NBS2, is required for activated defense responses in the *exo70B1* mutant. *PLoS Genetics*, **11**, e1004945.
- Zipfel, C. (2014) Plant pattern-recognition receptors. *Trends in Immunology*, **35**, 345–351.